Downloaded from rsta.royalsocietypublishing.org

PHILOSOPHICAL TRANSACTIONS OF THE ROYAL SOCIETY A MATHEMATICAL, PHYSICAL & ENGINEERING SCIENCES

Singularities Encountered in Three-Dimensional Boundary Layers under an Adverse or Favourable Pressure Gradient

S. N. Timoshin and F. T. Smith

Phil. Trans. R. Soc. Lond. A 1995 **352**, 45-87
doi: 10.1098/rsta.1995.0058

Email alerting service

Receive free email alerts when new articles cite this article - sign up in the box at the top right-hand corner of the article or click **here**

To subscribe to *Phil. Trans. R. Soc. Lond. A* go to:
http://rsta.royalsocietypublishing.org/subscriptions

This journal is © 1995 The Royal Society

Downloaded from rsta.royalsocietypublishing.org

Singularities encountered in three-dimensional boundary layers under an adverse or favourable pressure gradient

By S. N. Timoshin[1,2] and F. T. Smith[1]

[1] *Mathematics Department, University College, Gower Street, London WC1E 6BT, UK*

[2] *Central Aero-Hydrodynamical Institute, Zhukovsky-3, 140160, Russia*

Contents

Singularities in solutions of the classical boundary-layer equations are considered, numerically and analytically, in an example of steady hypersonic flow along a flat plate with three-dimensional surface roughness. First, a wide parametric study of the breakdown of symmetry-plane flow is performed for two particular cases of the surface geometry. Emphasis is put on the structural stability of the singularities' development to local/global variation of the pressure distribution. It is found that, as usual, the solution behaviour under an adverse pressure gradient involves the Goldstein- or marginal-type singularity at a point of zero streamwise skin friction. As the main alternative, typical of configurations with favourable or zero pressure forcing, an inviscid breakdown in the middle of the flow is identified. Similarly to unsteady flows, the main features of the novel singularity include infinitely growing boundary-layer thickness and finite limiting values of the skin-friction components. Subsequent analytical extensions of the singular symmetry-plane solution then suggest two different scenarios for the global boundary-layer behaviour: one implies inviscid breakdown of the flow at some singular line, the other describes the development of a boundary-layer collision at a downstream portion of the symmetry plane. In contrast with previous studies of the collision phenomenon in steady flows, the present theory suggests logarithmic growth of boundary-layer thickness on both sides of the discontinuity. Finally, an example of numerical solution of the full three-dimensional boundary layer equations is given. The flow régime chosen corresponds to inviscid breakdown of a centreplane flow under a favourable pressure gradient and

Phil. Trans. R. Soc. Lond. A (1995) **352**, 45–87
Printed in Great Britain

© 1995 The Royal Society

The Royal Society is collaborating with JSTOR to digitize, preserve, and extend access to *Philosophical Transactions: Physical Sciences and Engineering.*
www.jstor.org

Downloaded from rsta.royalsocietypublishing.org

development of the discontinuity/collision downstream. The numerical results near the origin of the discontinuity are found to be supportive, producing quantitative agreement with the local analytical description.

1. Introduction

(a) Background

The present article is aimed at further understanding of singularities encountered in solutions of the laminar steady three-dimensional boundary-layer (3-D BL) equations in the classical formulation, i.e. with the pressure gradient given in advance. The study is concentrated around special properties of 3-D BL flows stemming from the mixed parabolic–hyperbolic nature of their governing equations, the most remarkable of which are probably the occurrence of discontinuous solutions and the development of blow-up singularities.

The motivation for this work comes from the significant role of the classical BL concept in the modern theory of high-Reynolds-number fluid dynamics, especially in the theory of separated flows and, surprisingly enough, in the description of strongly nonlinear stages in laminar–turbulent transition. The subject has been quite widely discussed in original articles and monographs, and so just a few major applications of classical BLs are pointed out below. First, following Prandtl (1905), the classical BL approach is used in aerodynamics, biomechanics, geophysics, etc., as a fast and often accurate method for predicting dynamical and thermochemical properties of laminar viscous flows at large Reynolds numbers. Also, a number of existing empirical models allow for the properties of transitional/fully developed turbulent flows to be incorporated quite easily. In all these cases the 'attached BL strategy' is used, assuming that the solution can be obtained successively in the two major regions, those of the external inviscid flow and the thin viscous layer near the wall. The results tend to be in line with experimental observations and numerical solutions of the full Navier–Stokes equations, even at moderately large Reynolds numbers ($Re = 10^2$–10^3), but only for configurations sufficiently elongated in the streamwise direction, e.g. a flat plate without incidence (see Blasius 1908; Dennis & Chang 1969; Nishioka & Miyagi 1978). For more complicated geometries, the solution of the BL equations normally terminates at some singular point, or at a line in the 3-D case. (That is for the laminar régime, which is our main interest here; the attached-flow strategy tends to work even better for turbulent modelled BLs, as Prandtl and many references thereafter have pointed out (see, for example, Neish & Smith 1992)). Precise knowledge of the singular solutions is therefore necessary to organize the numerical process correctly and avoid mistreatments in the final results.

Second, the breakdown of the classical solution physically indicates: (*a*) the strong influence of separation/vortex shedding on the entire flow field; (*b*) a more complicated multi-zoned solution structure; (*c*) strong interaction between the viscous and inviscid flow, especially near separation/reattachment or corner points of the surface; and (*d*) even further complications caused by the generally observed transition of the detached shear layer, with additional large-scale or small-scale oscillations, 3-D vortical structures, and so on. As an alternative to the classical approach, the modern asymptotic treatment of high-Re flows suggests the 'viscous-inviscid interactive' strategy as a key, with features (*a–c*) above being taken into account through detailed description of all the asymptotic structure (see, for

PHILOSOPHICAL TRANSACTIONS OF THE ROYAL SOCIETY A MATHEMATICAL, PHYSICAL & ENGINEERING SCIENCES
PHILOSOPHICAL TRANSACTIONS OF THE ROYAL SOCIETY A MATHEMATICAL, PHYSICAL & ENGINEERING SCIENCES

Downloaded from rsta.royalsocietypublishing.org

example, review articles by Stewartson 1974, 1981, Neiland 1981, Smith 1982*a*, 1986 and the book by Sychev *et al.* 1987). The forecast with respect to point (*d*) above is also promising in view of the linear and nonlinear instabilities in separated flows (Brown *et al.* 1988; Smith 1986; Vickers 1992; Elliott & Smith 1987). In simplified versions of the interactive strategy, but based on a rigorous asymptotic description, a number of approximate sets of equations have been proposed for computing separated/transitional flows in various applications, at finite Reynolds numbers. The most successful models elaborate features (*a*, *c*, *d*), whereas computational efficiency often stems mainly from the diminished influence in the tiny asymptotic structure of the complex flow field (*b*) (see, for example, Davis & Werle 1982; Smith *et al.* 1984; Edwards 1987). Asymptotic theory has already explained rationally many major properties of steady and unsteady 2-D separations. However, it is felt that much more work is necessary in the 3-D case; for instance, the theory of open-type separation (Maskell 1955; Lighthill 1963) remains incomplete so far as its origins are concerned (but see Smith 1978). In this context an analysis of the classical solutions can reveal further useful guidelines towards the theory of fully 3-D BL separation.

Third, the link between the breakdown of the classical solution and the development of separated flow is not always evident. For, as a rule, the separation position has no direct relation with the position of singularities encountered in the attached strategy. However, in some special cases, with or without interaction, the classical theory does lead to correct prediction of the separation point. These cases are found in marginal-separation theory (see Stewartson *et al.* 1982; Ruban 1982*a*, and below) and in the study of the removable Goldstein singularity (Smith & Daniels 1981; Ruban 1990; Kerimbekov *et al.* 1994).

Our fourth point concerns a very significant application of the classical BL concept, namely in the fully nonlinear theory of laminar–turbulent transition, where, in contrast with linear and weakly nonlinear stages, complete alterations of the mean velocity profile are observed. Several different routes for transition have been identified, depending on the amplitude and frequency input conditions. Thus, for almost planar primary instability waves, nonlinear mechanisms typically come into operation with growing disturbance amplitude as in Smith & Burggraf (1985) (see also recent theoretical–experimental comparisons by Kachanov *et al.* (1993)). Simultaneously, a nonlinear viscous sublayer, governed by the classical BL formulation, develops closer to the solid surface. Its breakdown implies an additional eruption of vorticity into the main part of the BL, with subsequent splitting of the flow structure. Another example appears in nonlinear vortex–wave interaction, which is a typical product of the nonlinear development of 3-D instability waves. As shown in Smith & Walton (1989) and Walton & Smith (1992), for sufficiently long-scale perturbations the vortex motion is governed by the BL equations with known pressure gradient, the nonlinear interaction with the wave component then being incorporated in the boundary conditions. The last two papers mentioned then associate 3-D BL breakdown with the lift-off of lambda vortices that is often observed experimentally in deepening transition.

Finally here, a deeper understanding of the classical solutions can stimulate further work in the purely mathematical theory, especially concerning existence and uniqueness (as discussed in Nickel 1973, Telionis 1981 and Smith 1984), which can be vital for applications.

The fundamental properties of steady 3-D BL flow stem from the dual nature of

PHILOSOPHICAL TRANSACTIONS OF THE ROYAL SOCIETY A MATHEMATICAL, PHYSICAL & ENGINEERING SCIENCES

PHILOSOPHICAL TRANSACTIONS OF THE ROYAL SOCIETY A MATHEMATICAL, PHYSICAL & ENGINEERING SCIENCES

Downloaded from rsta.royalsocietypublishing.org

the governing equations – elliptic in the normal direction and hyperbolic in the directions tangential to the solid surface. This leads for instance to the existence of zones of influence and dependence in the form of curvilinear wedges with vertical boundaries (Raetz 1957; Wang 1971). Hence fairly standard restrictions on the initial velocity profile must be satisfied for the initial-boundary-value formulation to be well-posed (although our current work on instabilities in 3-D flows suggests that the above mentioned principle provides necessary, but not always sufficient, conditions for well-posedness). The mixed hyperbolic–elliptic type manifests itself also in the properties of singular classical solutions.

Some of the singularities have a direct counterpart in 2-D steady flow, being governed essentially by quasi-2-D dynamics. The most notable example here is the Goldstein singularity appearing under the influence of an adverse pressure gradient. Studied initially for 2-D flows (Goldstein 1948), it has also undoubtedly been identified in the 3-D case, both numerically (Wang 1970; Cebeci *et al.* 1980, 1981; Zametaev 1987*a*) and analytically (Brown 1965; Buckmaster 1972). The similarity between 2-D and 3-D flows persists to some extent also in the case of the weak Goldstein or marginal singularity. In the parametrically dependent 2-D flow, for example around an airfoil at slowly varying incidence, the marginal singularity naturally arises as an intermediate stage in the crossover from an ultimately regular solution to one with the Goldstein singularity (Werle & Davis 1972; Ruban 1981; Stewartson *et al.* 1982). The viscous–inviscid interaction that is inevitably present near the singular point provides an additional smoothing of the solution and, when viewed as a parametric process, describes also bifurcations/non-uniqueness in the flow with short separated bubbles (see Stewartson *et al.* 1982; Ruban 1982*a*, 1990; Brown & Stewartson 1983; Zametaev 1986). In the 3-D classical solution the marginal singularity can appear either at some line of the solid surface or at an isolated point. The first possibility has been studied for a self-similar flow, around a slender cone at incidence, by Zametaev (1987*a*). The solution properties turn out to be quite similar to those of the 2-D flow, including e.g. twofold continuation through the singular line. The resemblance vanishes, however, in the interaction region (Zametaev 1987*b*). The governing equation here acquires strong hyperbolic features, which make the whole description much more similar to the unsteady version of the 2-D theory in Smith (1982*b*) and Ruban (1982*b*). The isolated marginal singularity is related to the breakdown/separation in the symmetry plane of an elongated ellipsoid at incidence (Wang 1970; Cebeci *et al.* 1980). In that case, both the interactive and the classical solutions exhibit a strong influence of three-dimensionality (see Brown 1985; Duck 1989; Zametaev 1989).

Apart from affecting singularities which are mainly caused by an adverse pressure gradient (as above), the hyperbolic properties of the 3-D BL flow can themselves be responsible for the breakdown of the solution. This is evident for example in the classical problem of steady flow around a rapidly rotating sphere (Howarth 1951), where non-analytic behaviour is obtained in the form of a collision of two boundary layers at the equatorial plane. Similar collision occurs on the lee side of a conical body at incidence. A discontinuity/collision can also originate in a smooth solution as a result of gradually strengthening merging flow (in-flow) towards the centreplane. An example of this sort of breakdown is given in calculations of entry flow, in a curved duct, by Stewartson *et al.* (1980). Numerical results suggest first of all that the discontinuity originates through a strong blow-up singularity in the BL flow. The specific features of the singularity (unbounded BL thickness, zero limiting value of

PHILOSOPHICAL TRANSACTIONS OF THE ROYAL SOCIETY A MATHEMATICAL, PHYSICAL & ENGINEERING SCIENCES
PHILOSOPHICAL TRANSACTIONS OF THE ROYAL SOCIETY A MATHEMATICAL, PHYSICAL & ENGINEERING SCIENCES

Downloaded from rsta.royalsocietypublishing.org

the streamwise skin friction, etc.) were also verified, in an accompanying numerical and analytical study of the symmetry-plane solution ahead of breakdown, by Stewartson & Simpson (1982). Essentially the same singularity, but in a different context, is considered in Cebeci *et al.* (1983). Another suggestion derived from Stewartson *et al.* (1980) concerns the structure of the flow field downstream of the singularity: their numerical results indicate a regular distribution of the flow functions on approach to the discontinuity, or so it seems, with the limiting values of the cross velocity being finite but opposite in sign. This also implies a finite displacement thickness along the discontinuity. Similar conclusions were derived in the studies based on integral methods (Cousteix & Houdeville 1981) (but see the end of the present paper for alternative suggestions).

Further information, however, on the circumstances for the appearance of discontinuous solutions is rather scant. The collision in duct entry flow (above) develops under a very special pressure distribution; in particular, the streamwise pressure gradient is zero throughout the flow field. Also, the structure of the blow-up centreplane singularity is found to be strongly related to the local pressure distribution near the origin of the discontinuity. On the other hand, an exact solution for 3-D wall-jet flow illustrates the development of a collision without any influence of pressure forcing (Timoshin 1991). As a degenerate form of discontinuity, the collision can occur at an isolated point in flows with high symmetry, as in Brown & Simpson (1982) and Timoshin (1991).

One of the major objectives of the present article is to establish whether the occurrence of a discontinuity is a typical result of the general 3-D BL development and, if so, to provide the corresponding scenario of the BL breakdown. The particular flow geometry studied here is that of a hypersonic BL on a flat plate, with a small localized 3-D surface roughness. Apart from its importance for applications, this case seems to be very attractive for our purposes (see above), because the flow, which is governed by Ackeret pressure forces, allows both the local and the global external conditions to be changed easily without any loss of physical reality in the model. Thus, along with alterations in the local environment near any singularity, the influence of the flow history is also taken into account.

The plan of the paper is as follows. In §1*b* the flow geometry is specified and the initial-value/boundary-value problem governing the BL flow over the surface roughness is formulated. The flow is assumed to be symmetric with respect to the centreplane parallel to the freestream velocity. The analysis of the flow field starts in §2 with a numerical and analytical study of the typical symmetry-plane solutions. We consider first, in §2*a*, the limiting case of obstacles very narrow in the spanwise direction. The streamwise pressure gradient is zero in this limit, leading to a formulation similar to that of duct entry flow in Stewartson *et al.* (1980) but with much more freedom in the crosswise pressure distribution. As a result, in addition to the solution studied by Stewartson & Simpson (1982) and Cebeci *et al.* (1983), two more break-up singularities are identified. The position and specific form of the singularity are shown to be strongly dependent on the local pressure gradient, as well as on the flow development ahead of the breakdown. When the roughness width becomes finite, however, leading to a non-zero streamwise pressure gradient, the solution properties become quite different, as described in §2. First, only one of the above-mentioned break-up singularities is structurally stable to the streamwise pressure forcing now present. This singularity is purely inviscid and develops in the *middle* of the flow. It is remarkable, in fact, that the singularity can occur even in a

PHILOSOPHICAL TRANSACTIONS OF THE ROYAL SOCIETY A MATHEMATICAL, PHYSICAL & ENGINEERING SCIENCES

PHILOSOPHICAL TRANSACTIONS OF THE ROYAL SOCIETY A MATHEMATICAL, PHYSICAL & ENGINEERING SCIENCES

Downloaded from rsta.royalsocietypublishing.org

flow driven throughout by a *favourable* pressure gradient – a feature somewhat similar to the breakdown of 2-D and 3-D unsteady flows (Van Dommelen & Shen 1982; Elliott *et al.* 1983; Cowley *et al.* 1990; Van Dommelen & Cowley 1990; Peridier *et al.* 1991*a*, *b*). Second, because the flow typically contains regions with *adverse* pressure gradient, a breakdown of the Goldstein/marginal kind is generally expected, and indeed found, as an alternative. The main result of the symmetry-plane study, we believe, is the identification of the inviscid internal singularity and the Goldstein case as the two basic routes of 3-D boundary-layer breakdown.

In §3 we proceed to an asymptotic description of the singular solutions in the 3-D neighbourhood of the symmetry plane, when the breakdown in that plane is of the inviscid internal kind. The main goal there is to establish whether the break-up in the symmetry plane corresponds to the origin of a discontinuity downstream. We show, however, that the same symmetry-plane breakdown can occur in two completely different solutions of the full 3-D BL system. One of them terminates at a singular line, with an internal breakdown similar to that of 2-D steady flow on a downstream-moving surface (Sychev 1980; Elliott *et al.* 1983). The shape of this singular line is mostly regular but develops a cusp at the symmetry plane. The other local solution of the full 3-D equations is regular beside the symmetry plane and indeed describes effective collision of boundary layers. The form of collision is, we should stress, noticeably different from that proposed in Stewartson *et al.* (1980) and in particular the displacement thickness is unbounded on both sides of the discontinuity.

A numerical study of the full 3-D BL flow in one particular geometry (§4) is a culmination point of our analysis, because an appeal to the full formulation seems to be inevitable, first of all as a confirmation of the scenario (suggested in §3) of discontinuity development from an initially smooth solution. It also provides an independent check on the symmetry-plane study of §2. Further discussion, on the properties of the 3-D singular solutions and a number of suggestions stemming from our investigation, is given in §5.

(*b*) *Statement of the problem*

We consider 3-D hypersonic boundary-layer flow along a flat plate with a small localized 3-D surface roughness at a distance L^* from the leading edge. In the cartesian coordinates x^*, y^*, z^*, with x^* measured from the leading edge along the free stream and y^* normal to the plate, the shape of the roughness is described by the relation

$$y_w^* = L^* H f(x, z), \tag{1.1}$$

where local variables of order one in the region of the roughness are introduced as

$$x = \Delta^{-1}(x^*/L^* - 1), \quad z = \Delta^{-1} z^*/L^*, \tag{1.2}$$

and $\Delta \ll 1$ is the typical non-dimensional length scale of the roughness in both the streamwise and spanwise directions.

The thickening of the high-temperature boundary layer at large values of the free-stream Mach number M_∞ results in more intense interaction between the viscous and inviscid portions of the flow, which in turn leads to enhanced propagation of disturbances upstream of the surface irregularities (Lipatov 1980; Makhankov 1991). For a viscosity proportional to the absolute temperature and some standard conditions of heat transfer at the surface (e.g. prescribed temperature distribution), the length scale of the interaction region is estimated as

$$x^* - L^* = O(L^* Re^{-\frac{3}{8}} M_\infty^{\frac{9}{4}}), \tag{1.3}$$

Downloaded from rsta.royalsocietypublishing.org

where the Reynolds number is based on the free-stream parameters, $Re = \rho_\infty^* u_\infty^* L^*/\mu_\infty^*$. In particular, at sufficiently large Mach numbers $M_\infty = O(Re^{\frac{1}{6}})$ the interaction region will cover the entire flowfield between the leading edge and the roughness.

However, we are interested in the properties of the flow with a moderately large value of the Mach number and a sufficiently elongated shape of roughness, in which case effects of viscous–inviscid interaction and upstream propagation of disturbances may be neglected, to the leading approximation. This introduces the following restrictions on the orders of magnitude of the governing parameters:

$$1 \ll M_\infty \ll Re^{\frac{1}{6}}, \quad Re^{-\frac{3}{8}} M_\infty^{\frac{9}{4}} \ll \Delta \ll 1. \tag{1.4}$$

As usual for a locally perturbed boundary layer flow, the influence of viscosity is essential in a narrow wall layer only. Therefore the local flow field acquires a multi-layered structure including, along with the viscous sublayer, the passive major portion of the original flat-plate boundary layer and the outer region of potential flow. Under the restrictions (1.4) the latter region serves to provide the pressure distribution driving the flow in the viscous sublayer. If, in addition, the vertical scale of the surface roughness is sufficient to generate nonlinear perturbations in the wall region, the solution of the Navier–Stokes equations in the viscous sublayer has the following expansions:

$$\left.\begin{aligned}
&u^* = u_\infty^* \Delta^{\frac{1}{3}} \lambda_{\mathrm{w}}^{\frac{2}{3}} \mu_{\mathrm{w}}^{\frac{1}{3}} \rho_{\mathrm{w}}^{-\frac{1}{3}} u(x, y, z) + \dots,\\
&v^* - u^* \partial y_{\mathrm{w}}^*/\partial x^* - w^* \partial y_{\mathrm{w}}^*/\partial z^* = u_\infty^* M_\infty^2 Re^{-\frac{1}{2}} \Delta^{-\frac{1}{3}} \lambda_{\mathrm{w}}^{\frac{1}{3}} \mu_{\mathrm{w}}^{\frac{2}{3}} \rho_{\mathrm{w}}^{-\frac{2}{3}} v(x, y, z) + \dots,\\
&w^* = u_\infty^* \Delta^{\frac{1}{3}} \lambda_{\mathrm{w}}^{\frac{2}{3}} \mu_{\mathrm{w}}^{\frac{1}{3}} \rho_{\mathrm{w}}^{-\frac{1}{3}} w(x, y, z) + \dots,\\
&p^* = \rho_\infty^* u_\infty^{*2} [\gamma^{-1} M_\infty^{-2} + M_\infty^{-2} \Delta^{\frac{2}{3}} \lambda_{\mathrm{w}}^{\frac{4}{3}} \mu_{\mathrm{w}}^{\frac{2}{3}} \rho_{\mathrm{w}}^{\frac{1}{3}} p(x, z) + \dots],\\
&\rho^* = \rho_\infty^* M_\infty^{-2} \rho_{\mathrm{w}} + \dots, \quad \mu^* = \mu_\infty^* M_\infty^2 \mu_{\mathrm{w}} + \dots.
\end{aligned}\right\} \tag{1.5}$$

Here u^*, v^*, w^*, p^* denote the components of the velocity vector in the x^*, y^*, z^* directions and the pressure respectively, the superscript * refers to dimensional variables, and the free-stream values are marked with a subscript ∞. The main scaled parameters of the unperturbed boundary layer at the position of the roughness $x^* = L^*$, namely the skin friction and the density and viscosity at the wall, are denoted by λ_{w}, ρ_{w}, μ_{w} respectively. The vertical coordinate of order one in the wall region is defined by the relation

$$y^* - y_{\mathrm{w}}^* = L^* M_\infty^2 Re^{-\frac{1}{2}} \Delta^{\frac{1}{3}} \lambda_{\mathrm{w}}^{-\frac{1}{3}} \mu_{\mathrm{w}}^{\frac{1}{3}} \rho_{\mathrm{w}}^{-\frac{1}{3}} y. \tag{1.6}$$

Substitution of the expansions (1.5), (1.6) into the Navier–Stokes equations leads to the system of 3-D BL equations of an effectively incompressible fluid,

$$u\frac{\partial u}{\partial x} + v\frac{\partial u}{\partial y} + w\frac{\partial u}{\partial z} + \frac{\partial p}{\partial x} = \frac{\partial^2 u}{\partial y^2}, \tag{1.7a}$$

$$u\frac{\partial w}{\partial x} + v\frac{\partial w}{\partial y} + w\frac{\partial w}{\partial z} + \frac{\partial p}{\partial z} = \frac{\partial^2 w}{\partial y^2}, \tag{1.7b}$$

$$\frac{\partial u}{\partial x} + \frac{\partial v}{\partial y} + \frac{\partial w}{\partial z} = 0. \tag{1.7c}$$

The pressure forces in (1.7) are fixed by the Ackeret formula stemming from the analysis of the hypersonic flow outside the boundary layer, so that

$$p = h(\partial/\partial x) f(x, z), \tag{1.7d}$$

Downloaded from rsta.royalsocietypublishing.org

where the $O(1)$ parameter

$$h = H/(\Delta^{\frac{5}{3}} M_\infty^{-1} \lambda_w^{\frac{4}{3}} \mu_w^{\frac{2}{3}} \rho_w^{\frac{1}{3}}) \tag{1.8}$$

represents the scaled height of the roughness.

Boundary and initial conditions are those of no-slip at the solid surface and matching with the flow upstream and above the nonlinear viscous region. Thus

$$\text{at} \quad y = 0, \quad u = v = w = 0; \tag{1.9a}$$

$$\text{at} \quad x = 0, \quad u = y, \quad w = 0; \tag{1.9b}$$

$$\text{as} \quad y \to +\infty, \quad u - y \to A(x,z), \quad w \to 0. \tag{1.9c}$$

In (1.9b) it is assumed that the surface perturbations are absent for $x \leqslant 0$. The unknown function $-A(x,z)$ in (1.9c) is the normalized displacement thickness of the boundary layer.

Our concern, then, is with the solution properties of (1.7a–d) with (1.9a–c). As an example of the surface irregularity we consider a half-infinite dent defined by

$$f(x,z) = (1 - z^2/mb^2)^m \, (1 - (1 - \tfrac{1}{2}x)^4)^4, \quad |z| \leqslant b\sqrt{m} \quad \text{and} \quad 0 \leqslant x \leqslant 2; \tag{1.10a}$$

$$f(x,z) = (1 - z^2/mb^2)^m, \quad |z| \leqslant b\sqrt{m} \quad \text{and} \quad x \geqslant 2; \tag{1.10b}$$

and $f = 0$ elsewhere. The value of the parameter $m > 0$ is assumed to be large enough to provide smooth entry flow at the margins $z = \pm b\sqrt{m}$. Also the constant $b > 0$ and the value $b\sqrt{m}$ represents the half-width of the dent.

The case of a localized dent given by

$$f(x,z) = 4(1 - z^2/mb^2)^m \, (2x - x^2)^3, \quad |z| \leqslant b\sqrt{m} \quad \text{and} \quad 0 \leqslant x \leqslant 2, \tag{1.11}$$

was also considered in this research (with the same meaning of the parameters m, b), but just a few examples of the (symmetry-plane) solutions will be given below for (1.11). Our main example is that in (1.10a, b).

2. Solutions in the plane of symmetry

Both the numerical and the analytical treatment of the problem (1.7), (1.9) simplifies considerably in the symmetry plane of the boundary layer where the solution is independent of the rest of the flow. Assuming the shape of the roughness to be sufficiently smooth in z, we expand the solutions for (1.7), (1.9) in the usual manner, for small z:

$$\{u, v, w, p, f, A\} = \{u_0(x,y) + O(z^2), \quad v_0(x,y) + O(z^2), \quad z w_0(x,y) + O(z^3),$$
$$p_0(x) + z^2 p_1(x) + O(z^4), \quad f_0(x) + z^2 f_1(x) + O(z^4), \quad A_0(x) + O(z^2)\}, \tag{2.1}$$

yielding the boundary-value formulation for the leading terms in the following form:

$$u_0 \frac{\partial u_0}{\partial x} + v_0 \frac{\partial u_0}{\partial y} + \frac{\mathrm{d}p_0}{\mathrm{d}x} = \frac{\partial^2 u_0}{\partial y^2}, \tag{2.2a}$$

$$u_0 \frac{\partial w_0}{\partial x} + v_0 \frac{\partial w_0}{\partial y} + w_0^2 + 2p_1 = \frac{\partial^2 w_0}{\partial y^2}, \tag{2.2b}$$

$$\partial u_0/\partial x + \partial v_0/\partial y + w_0 = 0, \tag{2.2c}$$

$$p_0 = h \, \mathrm{d}f_0/\mathrm{d}x, \quad p_1 = h \, \mathrm{d}f_1/\mathrm{d}x, \tag{2.2d}$$

$$y = 0: \quad u_0 = v_0 = w_0 = 0; \quad x = 0: \quad u_0 = y, \quad w_0 = 0, \tag{2.2e,f}$$

$$y \to +\infty; \quad u_0 - y \to A_0(x), \quad w_0 \to 0. \tag{2.2g}$$

Downloaded from rsta.royalsocietypublishing.org

The problem above, although essentially 2-D, nevertheless reflects some important features of the original 3-D formulation, as mentioned in the Introduction. In particular, we have two components of the driving force – the pressure gradients streamwise and normal to the symmetry plane in (2.2*a*, *b*) respectively – that are almost independent in the case of locally perturbed hypersonic flow, according to (2.2*d*). Additional forcing of the streamwise flow, through the mass-conservation equation (2.2*c*), can be interpreted as an effect of contraction/expansion of the fluid particles surrounding the plane of symmetry.

A numerical solution for the problem (2.2*a*–*g*) could be obtained from a straightforward marching procedure based on, for example, a Crank–Nicolson approximation. Our test calculations, however, suggested that finite-distance singularities with unbounded thickening of the boundary layer were obtained, for various pressure distributions, resulting in substantial loss of accuracy close to the singular point. As might be expected, enlarging of the computational domain eventually led to excessive time- and memory-consuming calculations, the situation being very similar to those of the 2-D steady boundary layer on a moving wall (Telionis & Werle 1973; Williams & Johnson 1974; Zubarev 1983; Elliott *et al.* 1983) and the finite-time singularities in unsteady 2-D flows (for discussion and further references see Sychev *et al.* (1987), Van Dommelen & Cowley (1990) and Peridier *et al.* (1991*a*, *b*)).

Anticipating a mainly inviscid character for the singularities involving unbounded boundary-layer thickness, and taking also into account the analytical developments of Smith & Walton (1989) and Walton & Smith (1992), where the streamwise velocity component naturally arose as an independent variable in the local singular solutions, we obtained numerical and analytical results for the problem (2.2*a*–*g*) in Crocco variables. These are defined as

$$\xi = x, \quad \eta = u_0(x, y), \tag{2.3}$$

making use of the assumption of a monotonic streamwise velocity profile at any x-section, which is obviously satisfied at small x in view of the initial condition (2.2*f*); see also below for the comparison of the symmetry-plane results with those obtained in the global calculations of the 3-D flow in cartesian variables.

In Crocco variables (2.3) the problem (2.2*a*–*g*) reduces to the solution of two equations for the vorticity $\Omega = \partial u_0/\partial y$ and cross-velocity w_0 in the following form:

$$\eta \frac{\partial \Omega}{\partial \xi} - w_0 \Omega - \frac{\mathrm{d}p_0}{\mathrm{d}\xi} \frac{\partial \Omega}{\partial \eta} = \Omega^2 \frac{\partial^2 \Omega}{\partial \eta^2}, \tag{2.4a}$$

$$\eta \frac{\partial w_0}{\partial \xi} + w_0^2 - \frac{\mathrm{d}p_0}{\mathrm{d}\xi} \frac{\partial w_0}{\partial \eta} + 2p_1 = \Omega^2 \frac{\partial^2 w_0}{\partial \eta^2}, \tag{2.4b}$$

with the functions $p_0(\xi)$, $p_1(\xi)$ defined in (2.2*d*). The initial/boundary conditions following from (2.2*e*–*g*) and (2.2*a*) are:

$$\text{at} \quad \eta = 0, \quad w_0 = 0, \quad \Omega\, \partial\Omega/\partial\eta = \mathrm{d}p_0/\mathrm{d}\xi; \tag{2.5a}$$

$$\text{at} \quad \xi = 0, \quad \Omega = 1, \quad w_0 = 0; \tag{2.5b}$$

$$\text{as} \quad \eta \to +\infty, \quad \Omega \to 1, \quad w_0 \to 0. \tag{2.5c}$$

Downloaded from rsta.royalsocietypublishing.org

After the solution for (2.4) and (2.5) has been obtained, the normal velocity v_0 and vertical coordinate $y(\xi, \eta)$ may be calculated from the relations

$$v_0 = \eta \frac{\partial y}{\partial \xi} + \frac{\partial \Omega}{\partial \eta} - \Omega^{-1} \frac{\mathrm{d}p_0}{\mathrm{d}\xi}, \quad \frac{\partial y}{\partial \eta} = \frac{1}{\Omega} \tag{2.6a,b}$$

with the no-slip condition $y(\xi, \eta = 0) = 0$ used along with (2.6b). The relation

$$-A_0(\xi) = \lim_{\eta \to \infty} (y(\xi, \eta) - \eta) \tag{2.7}$$

enables the displacement thickness also to be evaluated afterwards.

The components of the pressure forces corresponding to the particular shapes of surface roughnesses (1.10a, b), (1.11) are evaluated as

$$p_0' = -12h(\tfrac{1}{2}x-1)^2[1-(\tfrac{1}{2}x-1)^4][1-5(\tfrac{1}{2}x-1)^4], \tag{2.8a}$$

$$p_1 = 8(h/b^2)(\tfrac{1}{2}x-1)^3[1-(\tfrac{1}{2}x-1)^4]^3, \tag{2.8b}$$

$$p'_0 = p_1 = 0, \quad x \geqslant 2 \quad \text{or} \quad x \leqslant 0, \tag{2.8c}$$

for the half-infinite dent (1.10), and similarly

$$p_0' = 24h(5x^2-10x+4)(2x-x^2), \tag{2.9a}$$

$$p_1 = -(h/b^2)\,24(1-x)(2x-x^2)^2, \tag{2.9b}$$

$$p_0' = p_1 = 0, \quad x \geqslant 2 \quad \text{or} \quad x \leqslant 0, \tag{2.9c}$$

for the localized dent (1.11). In both cases the width factor (b) of the obstacle appears only through the combination h/b^2 in the crosswise component of the pressure force, which naturally leads to the classification of the possible flow patterns in terms of two independent parameters, h and $h_w = h/b^2$. In particular, the limiting case $h_w \to 0$, $h = O(1)$ corresponds to quasi-2-D flows with well-established properties. More interesting for the purposes of the present paper, however, is the limit $h \to 0$, $h_w = O(1)$, corresponding to obstacles elongated in the streamwise direction. Similar régimes, but for different flow configurations, were studied earlier by Stewartson & Simpson (1982) and Cebeci, Stewartson & Brown (1983), hereinafter denoted by SS and CSB respectively.

(*a*) *Symmetry-plane solutions for elongated obstacles*

Some details of the numerical method applied in the solution of (2.4)–(2.7) are given in Appendix A.

We consider first the half-infinite obstacle giving the pressure gradient (2.8a–c) in the symmetry plane. In the limit $h \to 0$, $h_w = O(1)$, the only driving force appears as p_1 in the crosswise momentum equation. We notice further that p_1 is non-zero only in the interval $0 < x < 2$, with fluid being driven towards the symmetry plane if p_1 is positive (i.e. in the case of dent flow, $h_w < 0$) and outwards if p_1 is negative (hump flow with $h_w > 0$). Distributions of the streamwise skin friction $\tau_w = \partial u_0/\partial y$ $(x, y = 0)$, the displacement thickness $\delta_0 = -A_0(x)$ and the crosswise skin friction $\tau_z = \partial w_0/\partial y$ $(x, y = 0)$, for $h = 0$ and different values of $h_w = 0.45, -1.5, -0.9, -0.6, -0.5, -0.45$, are shown in figures 1–3 respectively.

Curves 1 in figures 1–3, corresponding to the boundary layer on a hump $h_w = 0.45$, represent an attached and smooth solution in the region considered. The pronounced maximum in τ_z suggests that strong 3-D vortical flow is generated in the adjustment region of the hump, i.e. $0 < x < 2$, but subsequent inertial development of the flow

Downloaded from rsta.royalsocietypublishing.org

Figure 1

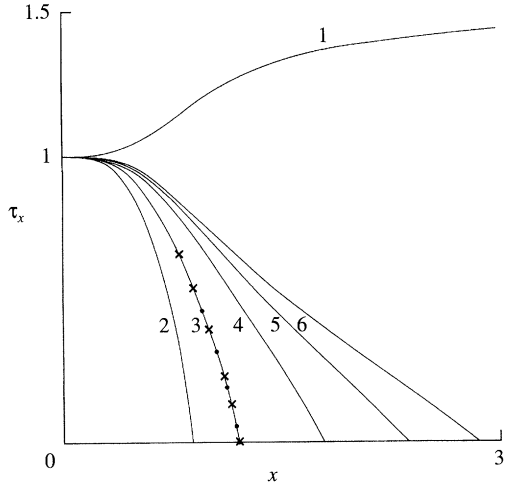

Figure 2

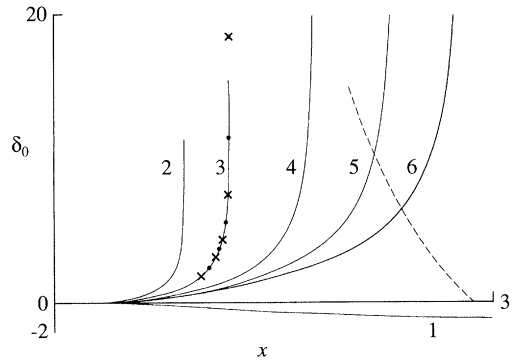

Figure 3

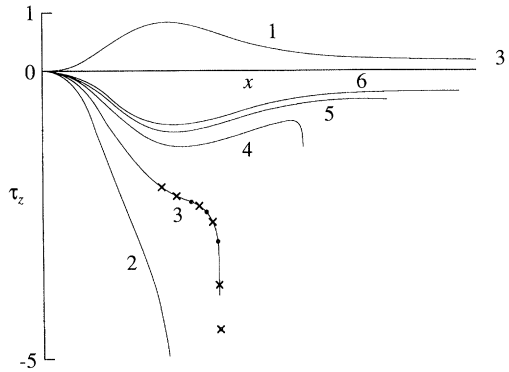

Figures 1–3. Calculated flow functions (in Crocco variables) plotted against x in the symmetry plane for the elongated half-infinite obstacle (1.10) with $h = 0$ and various finite $h_w = h/b^2$: figure 1, streamwise skin friction τ_x; figure 2, displacement thickness δ_0; figure 3, z-derivative of cross-flow skin friction τ_z. Curves 1–6 correspond to $h_w = 0.45, -1.5, -0.9, -0.6, -0.5, -0.45$, respectively. Grids used have various steps $\Delta\xi$, $\Delta\eta$, defined in Appendix A and various numbers of η-points N_η. Curve 1, $[\Delta\xi, \Delta\eta, N_\eta] = [0.01, 0.04, 300]$; (2), $[0.001, 0.02, 600]$; (3), $[0.001, 0.04, 600]$; 4–6, $[0.001, 0.04, 300]$. Influence of the grid in case 3: $\times$, $[0.001, 0.02, 600]$, $\bullet$, $[0.001, 0.04, 300]$. Dashed line in figure 2 represents the function $100\delta_0^{-\frac{3}{2}}$ for case 6; finite slope at the singular points is in agreement with (2.24).

field occurs in the region of zero pressure gradient $x > 2$, as can be seen from the behaviour of the streamwise skin friction and the displacement thickness.

Alteration of the sign of h_w causes dramatic changes in the flow properties. For the moderately deep dents (graphs 2 and 3 in figures 1–3), apparent breakdown of the solution is obtained at some point $x = x_s$ as a result of progressively enhancing inflow towards the centreplane. The most marked features of the suggested singular behaviour of the flow functions (the trends towards unbounded growth of the boundary-layer thickness δ_0, zero streamwise skin friction τ_x and infinitely large negative values of the crosswise skin friction τ_z) identify a singularity of the SS, CSB

Downloaded from rsta.royalsocietypublishing.org

kind, we believe. It was shown in the numerical and analytical treatment of SS, CSB, and also confirmed in our calculations, that the singularity develops in the near-wall region; this thickens infinitely in cartesian variables, owing to the mutually related deceleration and compression along the z-axis of the near-wall fluid particles. The majority of the boundary layer, therefore suffering just a vertical shift, has fairly passive dynamics.

From the above-mentioned papers, p_1 must be positive at the point of an SS–CSB singularity. We notice, however, from figures 1–3 that diminishing the depth of the dent leads to a downstream shift of the singular point (curves 2–4) until, eventually, the singularity is pushed into the region of constant pressure $x > 2$, where $p_1 = 0$ (curves 5 and 6). Then, although the qualitative behaviour of the displacement thickness and the skin friction τ_x remains unaltered (but notice the more regular approach of τ_x to zero now, from comparing curves 2 and 6 in figure 1), a *novel* structure of the singularities located at any $x = x_s > 2$ can be identified, or is suggested at least from the apparent finite limiting values of the crosswise skin friction τ_z in figure 3. Further illustration of the suggested new singular solution is given in figures 4–6, corresponding to $h = 0$, $h_w = -0.45$, in the form of the velocity and vorticity profiles near $x = x_s = 2.84$. The appearance of the minimum of vorticity at the wall in figure 4 (this minimum tends to zero as $x \to x_s$) indicates, as in SS, CSB, that the wall region which is narrow in Crocco variables is mainly responsible for the breakdown of the solution. This issue is also supported by the cross-velocity distributions in figure 5, the extremum of w_0 being shifted towards the wall closer to the singularity. Lastly, the enlarging (in y) linear portion of the streamwise velocity profile is evident in the wall region of figure 6.

We therefore next consider analytical properties of the near-wall singularity with zero pressure gradient, starting from the boundary-layer formulation (2.4)–(2.7). Based on the numerical results above, we expect the solution for w_0, Ω to be regular near $\xi(\equiv x) = \xi_s$ in the main portion of the flow, so that

$$\Omega = \Omega_0(\eta) + (\xi_s - \xi)\,\Omega_1(\eta) + \dots, \tag{2.10a}$$

$$w_0 = w_{00}(\eta) + (\xi_s - \xi)\,w_{01}(\eta) + \dots, \tag{2.10b}$$

where

$$\Omega_1 = -(\Omega_0 w_{00} + \Omega_0^2 \Omega_0'')/\eta, \quad w_{01} = (w_{00}^2 - \Omega_0^2 w_{00}'')/\eta \tag{2.11}$$

from (2.4a, b) respectively. In general, the leading terms of (2.10a, b) can be singular as $\eta \to 0$, say of the form

$$\Omega_0 = a\eta^{\alpha} + \dots, \quad w_{00} = -b\eta^{-\gamma} + \dots, \tag{2.12}$$

with constants $a, b, \alpha, \gamma > 0$, which is again consistent with the numerical results in figures 4 and 5. Then even stronger singularities will be obtained as $\eta \to 0$ in Ω_1, w_{01}, leading to the invalidity of the expansions (2.10a, b) in some narrow layer $\eta = O((\xi_s - \xi)^{\beta})$, with $\beta > 0$. Bearing in mind the sharply growing thickness of the boundary layer, we may suggest a nonlinear inviscid mechanism to remove the singularities in (2.10), (2.12) at $\eta = 0+$, leading therefore to an estimate $\beta = 1/(1+\gamma)$ and the additional restriction $2\alpha + \gamma > 2$ on the (unknown) α, γ values. In the nonlinear inviscid layer the solution is expanded as

$$\left.\begin{aligned} \Omega &= (\xi_s - \xi)^{\alpha/(\gamma+1)}\,\Omega_2(\mu) + \dots, \\ w_0 &= (\xi_s - \xi)^{-\gamma/(\gamma+1)}\,w_2(\mu) + \dots, \\ \mu &= \eta(\xi_s - \xi)^{-1/(\gamma+1)} = O(1), \end{aligned}\right\} \tag{2.13}$$

Downloaded from rsta.royalsocietypublishing.org

Figure 4

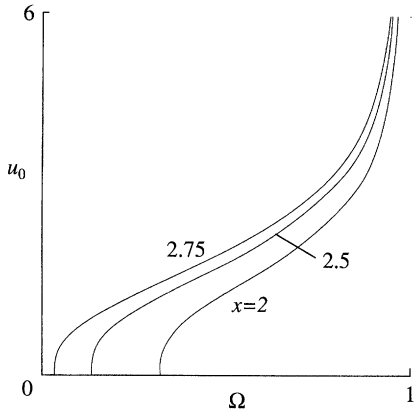

Figure 5

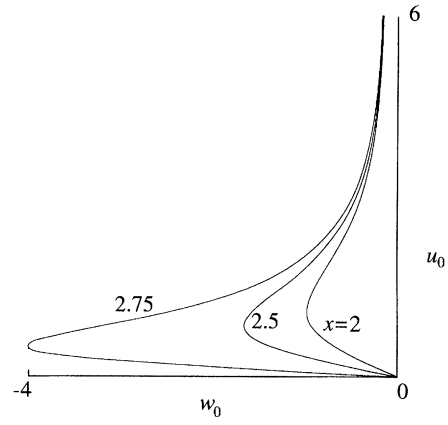

Figure 6

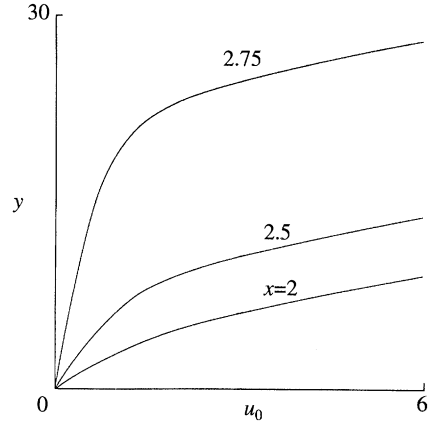

Figures 4–6. Development of the near-wall blow-up singularity under zero pressure gradient in centreplane solution corresponding to case 6 in figures 1–3, at three successive x-sections: figure 4, vorticity profiles $\Omega(u_0)$ in Crocco variables suggest minimum tending to zero at the wall; figure 5, pronounced minimum in z-derivative of the cross-velocity $w_0(u_0)$; figure 6, streamwise velocity profiles $u_0(y)$ reflect the growing BL thickness in cartesian variables.

with expressions for the leading terms satisfying matching conditions with (2.10), (2.12) of the form

$$\Omega_2 = a\mu^{\alpha-\gamma-1}(b+\mu^{\gamma+1}), \quad w_2 = -b\mu(b+\mu^{\gamma+1})^{-1}. \tag{2.14}$$

To complete the analysis and satisfy the no-slip conditions at the solid surface we consider next the viscous region defined by

$$\nu = \eta(\xi_s - \xi)^{-3/(5-2\delta)} = O(1), \quad \delta = \alpha - \gamma < \tfrac{5}{2}, \tag{2.15}$$

the latter restriction being necessary for the viscous region to be thin compared with the inviscid nonlinear zone. From (2.13)–(2.15), the leading approximation in the viscous region is

$$\Omega = (\xi_s - \xi)^{(2+\delta)/(5-2\delta)}\,\Omega_{30}(\nu) + \ldots, \quad w_0 = (\xi_s - \xi)^{(2\delta-2)/(5-2\delta)}\,w_{30}(\nu) + \ldots, \tag{2.16}$$

Downloaded from rsta.royalsocietypublishing.org

where the functions Ω_{30}, w_{30} must be determined as a solution of the nonlinear boundary-value problem

$$\Omega_{30}^2\Omega_{30}'' = \nu/(5-2\delta)\,[3\nu\Omega_{30}' - (2+\delta)\,\Omega_{30}] - w_{30}\Omega_{30}, \tag{2.17a}$$

$$\Omega_{30}^2 w_{30}'' = \nu/(5-2\delta)\,[3\nu w_{30}' - 2(\delta-1)\,w_{30}] + w_{30}^2, \tag{2.17b}$$

$$w_{30}(0) = \Omega_{30}'(0) = 0, \tag{2.17c}$$

$$\nu \to +\infty: \quad \Omega_{30} = ab\nu^{\delta-1} + \ldots, \quad w_{30} = -\nu + \ldots. \tag{2.17d}$$

An appropriate solution of (2.17*a–d*) is

$$\Omega_{30} = ab, \quad w_{30} = -\nu, \quad \delta = 1, \tag{2.18}$$

yielding, therefore, one relation between α and γ

$$\alpha - \gamma = 1. \tag{2.19}$$

We notice also that, in view of (2.15), (2.16), the relations (2.18) predict a finite value for the crosswise skin friction τ_z and a linear behaviour of the streamwise skin friction τ_x, which is in excellent agreement with our numerical results near the singular point.

Both α, γ are still arbitrary, related by means of (2.19) only. Considering the next terms in the expansion (2.16) we obtain

$$\Omega = (\xi_s - \xi)\,ab + (\xi_s - \xi)^{\alpha}\Omega_{31}(\nu) + \ldots, \tag{2.20a}$$

$$w_0 = -\nu + (\xi_s - \xi)^{\alpha-1} w_{31}(\nu) + \ldots. \tag{2.20b}$$

taking (2.18), (2.19) into account. The boundary-value formulation for the new terms is

$$a^2b^2w_{31}'' - \nu^2 w_{31}' + (\alpha+1)\,\nu w_{31} = 0, \tag{2.21a}$$

$$a^2b^2\Omega_{31}'' - \nu^2\Omega_{31}' + (\alpha-1)\,\nu\Omega_{31} = -abw_{31}, \tag{2.21b}$$

$$w_{31}(0) = \Omega_{31}'(0) = 0, \tag{2.21c}$$

$$\nu \to +\infty: \quad w_{31} = b^{-1}\nu^{\alpha+1} + \ldots, \quad \Omega_{31} = a\nu^{\alpha} + \ldots. \tag{2.21d}$$

As before, the conditions at infinity stem from the matching requirement with (2.13), (2.14). Substituting $t = \nu^3/(3a^2b^2)$, equations (2.21*a*, *b*) can be reduced to uniform and non-uniform confluent hypergeometric equations respectively. Appropriate solutions of (2.21*a–d*) then exist only if

$$\alpha = 3n, \quad n = 1, 2, \ldots, \tag{2.22}$$

in which case $w_{31}\,t^{-\frac{1}{3}}$ and Ω_{31} are just polynomial functions of t. If $n = 1$, for example, then

$$\alpha = 3, \quad w_{31} = b^{-1}(\nu^4 - 4a^2b^2\nu), \quad \Omega_{31} = a(\nu^3 - a^2b^2). \tag{2.23}$$

Thus an infinite number of singular solutions for the symmetry-plane equations (2.4*a*, *b*) can be obtained in a region of zero pressure gradient. However, the first of them, corresponding to $n = 1$, $\alpha = 3$, $\gamma = 2$, is likely to occur in the general case.

With α, γ given by (2.19), (2.22), the displacement thickness near the singular point is evaluated from (2.6*b*), (2.7) and (2.13) as

$$\delta_0 = -A_0(\xi) = \frac{1}{a}(\xi_s - \xi)^{(1/3n)-1} \int_0^{+\infty} \frac{\mathrm{d}s}{s^{3n}+b} + \ldots, \quad n = 1, 2, \ldots. \tag{2.24}$$

Downloaded from rsta.royalsocietypublishing.org

Figure 7

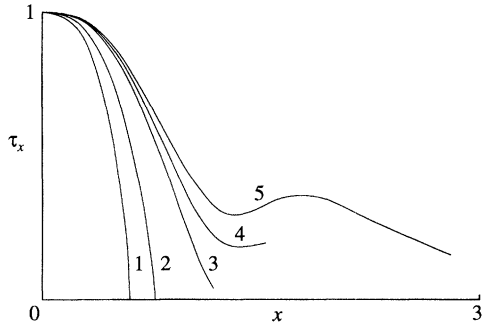

Figure 8

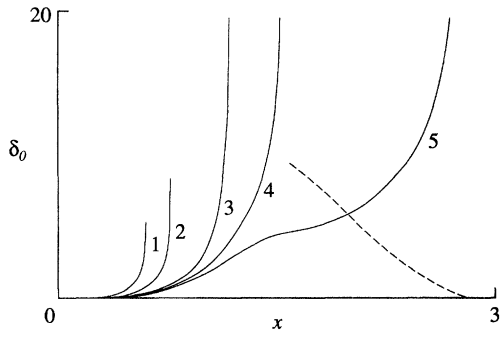

Figure 9

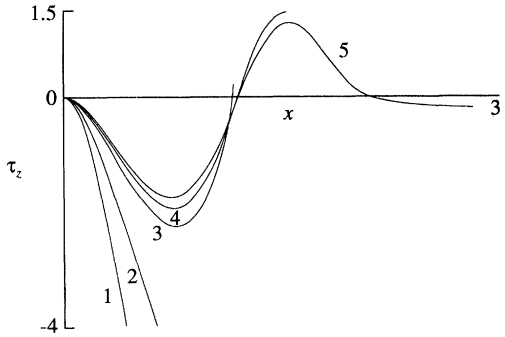

Figures 7–9. Calculated centreplane solutions (in Crocco variables) for the elongated localized dent (1.11) with $h = 0$, $h_w = h/b^2 = O(1)$: figure 7, streamwise skin friction τ_x: figure 8, displacement thickness δ_0; figure 9, z-derivative of cross-skin friction, plotted against x. Curves 1–5 are drawn for $h_w = -0.5, -0.3, -0.18, -0.16, -0.147$, respectively. Grids used have, for curve 1, $[\Delta\xi, \Delta\eta, N_\eta] = [0.002, 0.02, 600]$, and 2–5 [0.002, 0.04, 300]. Dashed line in figure 8 corresponds to $200\delta_0^{-2}$, case 5, with finite slope at the position of breakdown in agreement with (2.36).

It is remarkable that the major contribution to the displacement thickness is produced in the nonlinear inviscid region $\mu = O(1)$, whereas the viscosity is only responsible for the choice of eigenvalues in the local analysis. Further comparison of the asymptotic and numerical results is given in figure 2, where the dashed line reveals the linear behaviour of the function $\delta_0^{-\frac{3}{2}}$ on approach to the singular point. This is in good agreement with the value $n = 1$, $\delta_0 = O((\xi_s - \xi)^{-\frac{2}{3}})$ in (2.24), which also confirms our choice of $n = 1$ as the most general case.

Both SS–CSB and the singular solutions just described, although obtained in physically realistic configurations, nevertheless require very special local pressure distributions near the singular point. It turns out that another singularity, of a similar nature but structurally stable to the local pressure variation, develops in more general cases. It was first encountered in our symmetry-plane calculations for elongated localized obstacles, i.e. for the pressure gradient (2.9*a–c*) with $h \to 0$ and $h_w = h/b^2 = O(1)$. Corresponding results are shown in figures 7–9 for dent flows with $h = 0$, $h_w = -0.5, -0.3, -0.18, -0.16, -0.147$. Entry flow in a relatively deep dent (curves 1 and 2 in figures 7–9) yields the SS–CSB singularity until the singular point $x = x_s$ becomes located in the region of positive p_1, where $0 < x_s < 1$. For more shallow dents, $h_w > -0.2$, the singularity is shifted downstream to the interval $1 <$

Downloaded from rsta.royalsocietypublishing.org

Figure 10

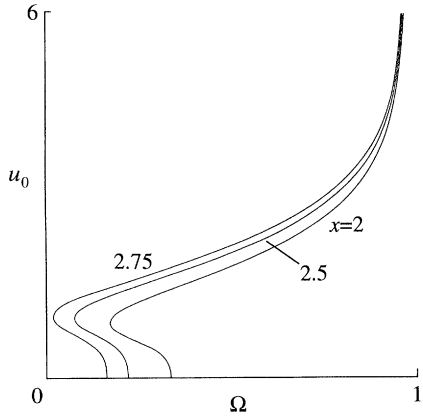

Figure 11

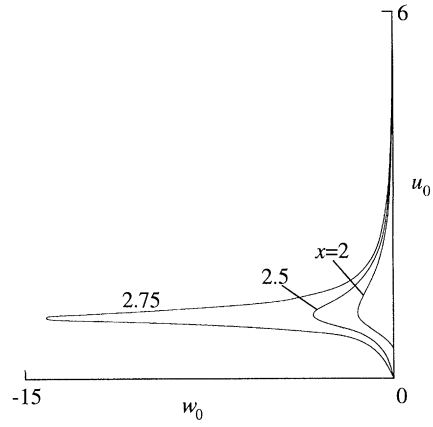

Figure 12

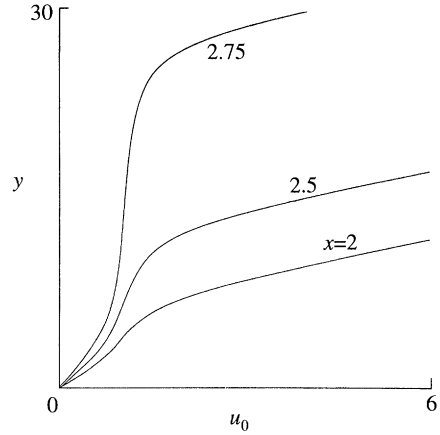

Figures 10–12. Vorticity and velocity distributions in the numerical solution corresponding to régime 5 in figures 7–9, at three x-sections ahead of the singularity. Breakdown in the middle of the flow terminates the solution in the region of zero pressure forcing $x > 2$, as can be seen from the development of an internal minimum in the vorticity profile $\Omega(u_0)$ (figure 10), the sharp peak in the derivative of the cross-velocity $w_0(u_0)$ (figure 11), and the plateau region in the streamwise velocity profile $u_0(y)$ (figure 12).

$x_s < 2$ with $p_1 < 0$. The apparently new character of the breakdown can be seen from the finite (and non-zero) limiting values of both components of the skin friction (figures 7 and 9) but still infinite displacement thickness (figure 8). It is remarkable also that qualitatively the same singularity persists for even shallower dents, where the singularity appears in the region of zero pressure gradient $x_s > 2$ (curves 5).

Thus, comparing figures 1–3 and figures 7–9 we conclude that both the local pressure distribution and the history of the boundary-layer development (i.e. global conditions) are responsible for the particular type of breakdown of the solution.

The behaviour of the vorticity and velocity components on approach to the singular point is shown in figures 10–12, corresponding to curves 5 in figures 7–9, $h = 0$, $h_w = -0.147$. The location of the minimum (tending to zero) in the vorticity distribution (figure 10), as well as the development of the plateau region in the

Downloaded from rsta.royalsocietypublishing.org

streamwise velocity profile (figure 12), undoubtedly indicates that internal processes *in the middle of the boundary layer* are dominant in this case. The analytical structure of the singularity in the middle of the flow is obtained from the symmetry-plane formulation (2.4)–(2.7) as follows. Consider for simplicity the case of zero local pressure gradient $\mathrm{d}p_0/\mathrm{d}x = p_1 = 0$, with further generalizations to be given in §3. Assume, as before, that the regular expansions (2.10*a*, *b*) hold true on approach to the singular point $\xi(=x) = \xi_s$ in the major portion of the boundary layer, but this time the limiting functions $\Omega_0(\eta)$, $w_{00}(\eta)$ are expected to be singular at some internal point $\eta = \eta_s > 0$, so that

$$\Omega_0 = a^{\pm}|\eta-\eta_s|^{\alpha}+\ldots, \quad w_{00} = -b^{\pm}|\eta-\eta_s|^{-\gamma}+\ldots. \tag{2.25}$$

Here $\eta-\eta_s \to \pm 0$ and the constants α, γ, $a^{\pm}$, $b^{\pm}$ are positive, in accordance with numerical results in figures 10 and 11. The singularities in (2.25) are removed in the collapsing layer where

$$\mu = (\eta-\eta_s)(\xi_s-\xi)^{-1/\gamma} = O(1), \quad \text{as} \quad \xi_s-\xi \to 0, \tag{2.26}$$

and, from matching with (2.25), the expansion for the flow function is

$$\Omega = (\xi_s-\xi)^{\alpha/\gamma}\Omega_2(\mu)+\ldots, \quad w_0 = (\xi_s-\xi)^{-1}w_2(\mu)+\ldots. \tag{2.27}$$

The additional assumption of a nonlinear and mainly inviscid nature of breakdown leads to the restriction $2\alpha+\gamma > 2$ on the eigenvalues α, γ and expressions for the coefficients in (2.27) of the form

$$\Omega_2 = (a^{\pm}/\eta_s)|\mu|^{\alpha-\gamma}(b^{\pm}+\eta_s|\mu|^{\gamma}), \quad w_2 = -b^{\pm}\eta_s(b^{\pm}+\eta_s|\mu|^{\gamma})^{-1}, \tag{2.28}$$

valid for $\mu > 0$ and $\mu < 0$ respectively.

The solution (2.27), (2.28) is still singular at $\mu = 0$; hence we consider a viscous sublayer and define

$$\nu = (\eta-\eta_s)(\xi_s-\xi)^{-\frac{3}{2}(1-\delta)} = O(1), \quad \text{as} \quad \xi_s-\xi \to 0, \quad \text{with} \quad \delta = \alpha-\gamma < 1. \tag{2.29}$$

The leading terms of the solution in this viscous region are

$$\Omega = (\xi_s-\xi)^{(2+\delta)/(2(1-\delta))}\Omega_{30}(\nu)+\ldots, \quad w_0 = (\xi_s-\xi)^{-1}w_{30}(\nu)+\ldots. \tag{2.30}$$

The functions Ω_{30}, w_{30} then satisfy the boundary-value formulation

$$\Omega_{30}^2\Omega_{30}'' = [\eta_s/2(1-\delta)][3\nu\Omega_{30}'-(2+\delta)\Omega_{30}]-w_{30}\Omega_{30}, \tag{2.31a}$$

$$\Omega_{30}^2 w_{30}'' = \eta_s\{[3\nu/2(1-\delta)]w_{30}'+w_{30}\}+w_{30}^2, \tag{2.31b}$$

such that, as $\nu \to \pm\infty$,

$$\Omega_{30} = (a^{\pm}b^{\pm}/\eta_s)|\nu|^{\delta}+\ldots, \quad w_{30} = -\eta_s+\ldots, \tag{2.31c}$$

where matching conditions with (2.27), (2.28) are taken into account. The appropriate solution of (2.31*a*–*c*) is therefore

$$\Omega_{30} = a^+b^+/\eta_s = a^-b^-/\eta_s, \quad w_{30} = -\eta_s, \quad \delta = 0, \tag{2.32}$$

giving in particular the relation $\alpha = \gamma$ in view of (2.29).

The eigenvalues α,γ are finally determined from considering further terms in the expansions (2.30), namely

$$\Omega = (\xi_s-\xi)a^+b^+/\eta_s+\ldots+(\xi_s-\xi)^{\frac{3}{2}\alpha}\Omega_{31}(\nu)+\ldots, \tag{2.33a}$$

$$w_0 = -(\xi_s-\xi)^{-1}\eta_s+\ldots+(\xi_s-\xi)^{\frac{3}{2}\alpha-2}w_{31}(\nu)+\ldots, \tag{2.33b}$$

Downloaded from rsta.royalsocietypublishing.org

yielding the boundary-value formulation for Ω_{31}, w_{31} in the form

$$(a^+b^+/\eta_s)^2\Omega''_{31} = \tfrac{3}{2}\eta_s(\nu\Omega'_{31} - \alpha\Omega_{31}) - (a^+b^+/\eta_s)\,w_{31} + \eta_s\,\Omega_{31}. \tag{2.34a}$$

$$(a^+b^+/\eta_s)^2 w''_{31} = \tfrac{1}{2}\eta_s(3\nu w'_{31} - (3\alpha - 4)\,w_{31}) - 2\eta_s\,w_{31}, \tag{2.34b}$$

with, as $\nu \to \pm\infty$, $w_{31} = (\eta_s^2/b^\pm)\,|\nu|^\alpha + \ldots$, $\Omega_{31} = a^\pm|\nu|^\alpha + \ldots$. (2.34c)

Regular solutions of (2.34*a–c*) are necessarily polynomial functions of ν, a result that can be established by, for example, taking appropriate derivatives of (2.34*a*, *b*) and then applying Fourier transformation in ν. This gives, for positive $a^\pm$, $b^\pm$ (see also (2.25)), an infinite number of eigenvalues

$$\alpha = \gamma = 2n, \quad n = 1, 2 \ldots \tag{2.35}$$

and also the two relations $a^+ = a^-$, $b^+ = b^-$.

The infinite spectrum of possible internal singular solutions of the symmetry-plane equations can be further characterized by the local displacement-thickness growth as

$$\delta_0 = (\xi_s - \xi)^{(1/2n)-1}\,\frac{\eta_s}{a^+}\int_{-\infty}^{\infty}\frac{\mathrm{d}\mu}{b^+ + \eta_s\,\mu^{2n}} + \ldots, \quad \text{for} \quad n = 1, 2, \ldots, \tag{2.36}$$

from (2.7), (2.26)–(2.28). In a numerical solution the case $n = 1$ is observed typically, as can be seen from the finite slope of the function $\delta_0(x)^{-2}$ at the singular point (the dashed line in figure 8).

(*b*) *Symmetry-plane solutions for finite-width obstacles*

To study the influence of non-zero streamwise pressure gradient on the breakdown of symmetry-plane flow we consider below examples of the numerical solution of (2.4)–(2.7) for the half-infinite surface roughness, where the pressure gradient is given in (2.8*a–c*). The case of relatively narrow roughness $b = 0.2$ was chosen to (roughly) estimate the physical relevance of the above limit of an infinitely narrow configuration $h = 0$, $h_w = h/b^2 = O(1)$.

Graphs of the streamwise skin friction τ_x and displacement thickness δ_0 are shown in figures 13 and 14 respectively, for the range of the depth/height parameter $h = -1$, -0.4, -0.1, -0.03, -0.02, 0.2, 0.335, 0.36. Considering first the dent flow ($h < 0$), we notice that the streamwise pressure gradient (2.8*a*) is favourable in the entry portion of the dent $0 < x < x_0 = 2(1 - 5^{-\frac{1}{4}}) = 0.6625$ but adverse in the region $x_0 < x < 1$. Influenced by additional accelerating/decelerating pressure forcing, the SS–CSB singularity of the highly elongated limit (figures 1–3) is now replaced by one of the two more stable structures, either that described in (2.25)–(2.36) or the Goldstein structure. Thus, if the breakdown occurs in the region $0 < x_s < x_0$, the singularity develops in the middle of the flow (curves 1 and 2 in figures 13 and 14), as can be seen from the unbounded growth of the boundary-layer thickness but with regular behaviour of the streamwise skin friction. In contrast, the Goldstein singularity, typical of boundary layers with adverse pressure gradient, is observed in the interval $x_0 < x_s < 2$ (see curves 3 and 4). For a sufficiently shallow dent the singular point is shifted downstream of the adjustment region $x_s > 2$ (curves 5). Active pressure forcing is absent here, leading thereby to the development of a near-wall singularity the same as for the limit $h \to 0$ in figures 1–3.

As regards the hump flows ($h > 0$), the properties of the solution turn out to be qualitatively close to those of 2-D and previously studied 3-D flows. With increasing height of the hump (curves 6–8) the solution transforms from fully attached to

PHILOSOPHICAL TRANSACTIONS OF THE ROYAL SOCIETY A MATHEMATICAL, PHYSICAL & ENGINEERING SCIENCES
PHILOSOPHICAL TRANSACTIONS OF THE ROYAL SOCIETY A MATHEMATICAL, PHYSICAL & ENGINEERING SCIENCES

Downloaded from rsta.royalsocietypublishing.org

Figure 13

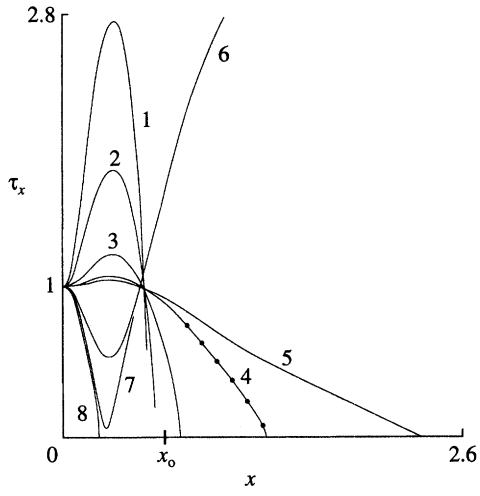

Figure 14

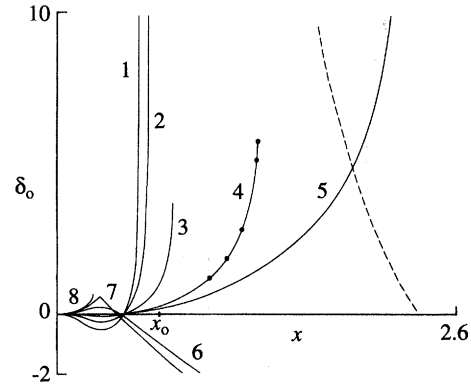

Figures 13 and 14. Calculated centreplane flow functions for the half-infinite roughness (1.10) of finite width $b = 0.2$, $m = 4$: figure 13, streamwise skin friction τ_x; figure 14, displacement thickness δ_0 plotted against x. Curves 1–8 are drawn for values of the height/depth parameter $h = -1$, -0.4, -0.1, -0.03, -0.02, 0.2, 0.335, 0.36, respectively. Grids used in Crocco variables have, for case 1, $[\Delta\xi, \Delta\eta, N_\eta] = [0.0001, 0.02, 600]$; 2, [0.0002, 0.02, 600]; 3, [0.0005, 0.02, 600]; 4, [0.01, 0.04, 300]; 5, [0.001, 0.04, 300]; 6 and ●, [0.001, 0.02, 600]; 7, 8, [0.001, 0.02, 300]. The calculations suggest two possible singularities in the region of non-zero streamwise pressure gradient $0 < x < 2$: the Goldstein/marginal as in cases 3, 4, 7, 8, or internal inviscid as in 1, 2. The dashed line in figure 14 drawn for $50\delta_0^{-\frac{3}{2}}$, case 5, confirms the same as in figures 1–6, namely near-wall blow-up singularity without active pressure forcing.

marginally singular and, finally, to the solution with a Goldstein singularity (see Werle & Davis 1972; Ruban 1981, 1982*a*; Stewartson *et al.* 1982; Cebeci *et al.* 1980; Brown 1985; Zametaev 1987*a*, 1989).

The breakdown described above for a steady attached boundary layer in a region of *favourable* pressure gradient is a remarkable event and deserves further investigation. In §§3 and 4 below we present the results of analytical and numerical treatments of the complete 3-D boundary layer, for cases containing the inviscid internal singularity in the corresponding symmetry-plane solution above. It will be shown that the hyperbolic properties of the 3-D boundary layer are mainly responsible for this kind of breakdown, with the intersection of characteristics and the formation of shock-like discontinuities (or alternatively envelopes) being the major global issue.

3. Inviscid singularities in the vicinity of the symmetry plane

Although the appearance of singularities in the symmetry-plane solution strongly indicates breakdown of the initially attached boundary layer, further analysis is necessary to clarify the nature of the singularity in the global 3-D flow. We derive below the analytical 3-D extension of the solution with an inviscid internal singularity in (2.25)–(2.36) for the immediate neighbourhood of the plane of symmetry. To demonstrate the applicability of our results to other incompressible

Downloaded from rsta.royalsocietypublishing.org

flows we consider the general case of a 3-D boundary layer on an arbitrary smooth surface governed by the equations (see, for example, Crabtree *et al.* 1963)

$$\frac{u}{h_1}\frac{\partial u}{\partial x}+v\frac{\partial u}{\partial y}+\frac{w}{h_2}\frac{\partial u}{\partial z}+\frac{uw}{h_1h_2}\frac{\partial h_1}{\partial z}-\frac{w^2}{h_1h_2}\frac{\partial h_2}{\partial x}+\frac{1}{h_1}\frac{\partial p}{\partial x}=\frac{\partial^2 u}{\partial y^2}, \tag{3.1a}$$

$$\frac{u}{h_1}\frac{\partial w}{\partial x}+v\frac{\partial w}{\partial y}+\frac{w}{h_2}\frac{\partial w}{\partial z}+\frac{uw}{h_2h_2}\frac{\partial h_2}{\partial x}-\frac{u^2}{h_1h_2}\frac{\partial h_1}{\partial z}+\frac{1}{h_2}\frac{\partial p}{\partial z}=\frac{\partial^2 w}{\partial y^2}, \tag{3.1b}$$

$$\frac{1}{h_1}\frac{\partial u}{\partial x}+\frac{\partial v}{\partial y}+\frac{1}{h_2}\frac{\partial w}{\partial z}+\frac{u}{h_1h_2}\frac{\partial h_2}{\partial x}+\frac{w}{h_1h_2}\frac{\partial h_1}{\partial z}=0. \tag{3.1c}$$

Here the Lamé coefficients $h_1(x,z)$, $h_2(x,z)$ and the prescribed pressure $p(x,z)$ are all regular functions of x,z, and also some standard initial and boundary conditions are assumed for the unknown velocity components u, v, w, along the x, y, z axes respectively.

As before, the analysis can be somewhat simplified if, instead of the normal coordinate y, a new variable is introduced which remains of order one in a thickening boundary layer. For easier interpreting of the final results we choose the stream function $\psi=\psi(x,y,z)$ as the new variable. The monotonicity of ψ as a function of y at any fixed x, z is, of course, very unlikely in a general 3-D boundary layer. However, in the local solution below we verify this condition, which is obviously satisfied in the symmetry plane upstream of the singular point. In the new variables x,ψ,z we obtain from (3.1*a–c*) the three equations

$$\frac{u}{h_1}\frac{\partial u}{\partial x}+\frac{w}{h_2}\frac{\partial u}{\partial z}+\frac{uw}{h_1h_2}\frac{\partial h_1}{\partial z}-\frac{w^2}{h_1h_2}\frac{\partial h_2}{\partial x}+\frac{1}{h_1}\frac{\partial p}{\partial x}=\frac{1}{r}\frac{\partial}{\partial\psi}\left(\frac{1}{r}\frac{\partial u}{\partial\psi}\right), \tag{3.2a}$$

$$\frac{u}{h_1}\frac{\partial w}{\partial x}+\frac{w}{h_2}\frac{\partial w}{\partial z}+\frac{uw}{h_1h_2}\frac{\partial h_2}{\partial x}-\frac{u^2}{h_1h_2}\frac{\partial h_1}{\partial z}+\frac{1}{h_2}\frac{\partial p}{\partial z}=\frac{1}{r}\frac{\partial}{\partial\psi}\left(\frac{1}{r}\frac{\partial w}{\partial\psi}\right), \tag{3.2b}$$

$$(\partial/\partial x)\,(ruh_2)+(\partial/\partial z)\,(rwh_1)=0, \tag{3.2c}$$

governing the velocity components u, w tangential to the solid surface and the function $r(x,\psi,z)$, which is defined by

$$r(x,\psi,z)=\partial y(x,\psi,z)/\partial\psi \tag{3.2d}$$

and, once known, serves for evaluating the vertical coordinate $y(x,\psi,z)$. The additional relation for the vertical velocity

$$v(x,\psi,z)=\frac{u}{h_1}\frac{\partial y}{\partial x}+\frac{w}{h_2}\frac{\partial y}{\partial z}, \tag{3.2e}$$

stems from the definition of the streamfunction.

With $z=0$ being the symmetry plane, we expand the solution for (3.2*a–c*) upstream of the singular point in power series in z of the form:

$$u=u_0(x,\psi)+z^2u_1(x,\psi)+\ldots,\quad w=zw_0(x,\psi)+z^3w_1(x,\psi)+\ldots, \tag{3.3a,b}$$

$$r=r_0(x,\psi)+z^2r_1(x,\psi)+\ldots,\quad p=p_0(x)+z^2p_1(x)+z^4p_2(x)\ldots, \tag{3.3c,d}$$

$$h_1=h_{10}(x)+z^2h_{11}(x)+z^4h_{12}(x)+\ldots,\quad h_2=h_{20}(x)+z^2h_{21}(x)+z^4h_{22}(x)+\ldots. \tag{3.3e,f}$$

Downloaded from rsta.royalsocietypublishing.org

Considering first the leading approximations in (3.3*a–f*), we obtain from (3.2*a–c*) the system of equations for the symmetry-plane motion:

$$\frac{u_0}{h_{10}}\frac{\partial u_0}{\partial x}+\frac{1}{h_{10}}\frac{\mathrm{d}p_0}{\mathrm{d}x}=\frac{1}{r_0}\frac{\partial}{\partial\psi}\left(\frac{1}{r_0}\frac{\partial u_0}{\partial\psi}\right), \tag{3.4a}$$

$$\frac{u_0}{h_{10}}\frac{\partial w_0}{\partial x}+\frac{w_0^2}{h_{20}}+\frac{u_0 w_0}{h_{10}h_{20}}\frac{\mathrm{d}h_{20}}{\mathrm{d}x}-\frac{2u_0^2 h_{11}}{h_{10}h_{20}}+\frac{2p_1}{h_{20}}=\frac{1}{r_0}\frac{\partial}{\partial\psi}\left(\frac{1}{r_0}\frac{\partial w_0}{\partial\psi}\right), \tag{3.4b}$$

$$(\partial/\partial x)\,(u_0 r_0 h_{20})+r_0 w_0 h_{10}=0. \tag{3.4c}$$

For a flat surface ($h_1=h_2=1$) the system (3.4*a–c*) is equivalent to the previously studied equations (2.4*a*, *b*). We may therefore derive from (3.4*a–c*) the description of the inviscid singularity in the middle of the flow in a manner similar to that in the previous section, with minor changes caused by the curvature properties of the solid surface. The general structure of the singular solution could be seen easily from a qualitative analysis as follows. Assume that on approach to the singularity (say as $x\to-0$) the boundary-layer thickness tends to infinity, owing to the compression in the cross-direction of fluid particles corresponding to $\psi\approx\psi_0>0$. If the streamwise velocity of the compressed particles remains finite and non-zero then the enhancing of the displacement effect (which means $r_0\to+\infty$) must be supported by an unbounded growth of $|w_0|$. Assuming also that the process described is predominantly inviscid, we obtain from (3.4*b*, *c*) two approximate equations, valid in the compression region $|\psi-\psi_0|\ll 1$, $|x|\ll 1$, of the form:

$$\frac{u_0(0,\psi_0)}{h_{10}(0)}\frac{\partial w_0}{\partial x}+\frac{w_0^2}{h_{20}(0)}=0, \tag{3.5a}$$

$$u_0(0,\psi_0)\,h_{20}(0)\frac{\partial r_0}{\partial x}+h_{10}(0)\,r_0\,w_0=0. \tag{3.5b}$$

The general solution for (3.5*a*, *b*) containing arbitrary functions $g_1(\psi)$, $g_2(\psi)$ is

$$w_0=-\frac{h_{20}(0)\,u_0\,(0,\psi_0)}{h_{10}(0)\;\;[g_1(\psi)-x]},\quad r_0=\frac{g_2(\psi)}{g_1(\psi)-x}. \tag{3.6a, b}$$

In this local analysis the leading terms of the series representation for g_1, g_2 near $\psi=\psi_0$ are informative on their own. Together with the requirement of regularity for $x<0$ and also smoothness properties of g_1, g_2 (following basically from the inviscid character of the singularity), this leads to the estimates $g_1\sim(\psi-\psi_0)^2$, $g_2=\text{const.}$ The displacement thickness, proportional to $(-x)^{-\frac{1}{2}}$, is obtained now from (3.6*b*) taking (3.2*d*) into account.

The description above, which is in line with the results of the previous section, can easily be formalized in terms of asymptotic expansions for the solution of (3.4*a–c*) as $x\to-0$. The corresponding multi-layered structure near $x=0$ includes two passive layers above and below $\psi=\psi_0$, with regular expansions for u_0, w_0, r_0 in powers of $-x$, and also a collapsing locally inviscid zone defined by

$$\eta=(\psi-\psi_0)\,(-x)^{-\frac{1}{2}}=O(1),\quad \xi=-x\to 0. \tag{3.7}$$

Making use of Taylor expansions for the known functions (with the tensor summation rule) of the form

$$h_1=a_{ij}z^{2i}x^j,\quad h_2=b_{ij}z^{2i}x^j,\quad p=p_{ij}z^{2i}x^j,\quad i,j=0,1,\ldots, \tag{3.8}$$

Downloaded from rsta.royalsocietypublishing.org

the solution in the inviscid zone (3.7) is expanded as

$$u_0 = \bar{u}_0 + \xi^{\frac{1}{2}}\bar{u}_1(\eta) + \ldots, \tag{3.9a}$$

$$w_0 = \xi^{-1}\bar{w}_0(\eta) + \xi^{-\frac{1}{2}}\bar{w}_1(\eta) + \ldots, \tag{3.9b}$$

$$r_0 = \xi^{-1}\bar{r}_0(\eta) + \ldots, \tag{3.9c}$$

where

$$\bar{w}_0 = -(b_{00}\,\bar{u}_0/a_{00})\,[c_0/(c_0+\eta^2)], \tag{3.10a}$$

$$\bar{w}_1 = \frac{c_1\eta^3}{(c_0+\eta^2)^2} - \frac{b_{00}\,c_2\,c_0^2}{a_{00}}\frac{\eta}{(c_0+\eta^2)^2}, \tag{3.10b}$$

$$\bar{u}_1 = c_2\,\eta, \tag{3.10c}$$

$$\bar{r}_0 = (d_0/\bar{u}_0\,b_{00})\,[c_0/(c_0+\eta^2)]. \tag{3.10d}$$

The constants $\bar{u}_0$, a_{00}, b_{00}, c_0, c_2, d_0 in (3.10*a–d*) are all positive.

Consider now the next approximation in the expansions (3.3). The equations for the unknown functions u_1, w_1, r_1 are, from (3.2*a–c*),

$$u_0\frac{\partial u_1}{\partial x} + u_1\frac{\partial u_0}{\partial x} + 2\frac{h_{10}}{h_{20}}u_1\,w_0 + 2\frac{h_{11}}{h_{20}}u_0\,w_0 - \frac{w_0^2}{h_{20}}\frac{\mathrm{d}h_{20}}{\mathrm{d}x} + \frac{\mathrm{d}p_1}{\mathrm{d}x}$$
$$= \frac{h_{10}}{r_0}\frac{\partial}{\partial\psi}\left(\frac{1}{r_0}\frac{\partial u_1}{\partial\psi} - \frac{r_1}{r_0^2}\frac{\partial u_0}{\partial\psi}\right) + \left(\frac{h_{11}}{r_0} - \frac{h_{10}\,r_1}{r_0^2}\right)\frac{\partial}{\partial\psi}\left(\frac{1}{r_0}\frac{\partial u_0}{\partial\psi}\right), \tag{3.11a}$$

$$u_0\frac{\partial w_1}{\partial x} + u_1\frac{\partial w_0}{\partial x} + 4\frac{h_{10}}{h_{20}}w_0\,w_1 + w_0^2\left(\frac{h_{11}}{h_{20}} - \frac{h_{10}\,h_{21}}{h_{20}^2}\right) + \frac{1}{h_{20}}(u_0\,w_1 + u_1\,w_0)\frac{\mathrm{d}h_{20}}{\mathrm{d}x}$$
$$+ \left(\frac{1}{h_{20}}\frac{\mathrm{d}h_{21}}{\mathrm{d}x} - \frac{h_{21}}{h_{20}^2}\frac{\mathrm{d}h_{20}}{\mathrm{d}x}\right)u_0\,w_0 - u_0^2\left(\frac{4h_{12}}{h_{20}} - \frac{2h_{11}\,h_{21}}{h_{20}^2}\right) - \frac{4h_{11}}{h_{20}}u_0\,u_1$$
$$+ \frac{4h_{10}}{h_{20}}p_2 + 2\left(\frac{h_{11}}{h_{20}} - \frac{h_{10}\,h_{21}}{h_{20}^2}\right)p_1$$
$$= \frac{h_{10}}{r_0}\frac{\partial}{\partial\psi}\left(\frac{1}{r_0}\frac{\partial w_1}{\partial\psi} - \frac{r_1}{r_0^2}\frac{\partial w_0}{\partial\psi}\right) + \left(\frac{h_{11}}{r_0} - \frac{h_{10}\,r_1}{r_0^2}\right)\frac{\partial}{\partial\psi}\left(\frac{1}{r_0}\frac{\partial w_0}{\partial\psi}\right), \tag{3.11b}$$

$$\frac{\partial}{\partial x}[u_0\,r_0\,h_{21} + h_{20}(r_0\,u_1 + r_1\,u_0)] + 3[r_0\,h_{10}\,w_1 + w_0\,r_0\,h_{11} + w_0\,r_1\,h_{10}] = 0. \tag{3.11c}$$

In the inviscid zone (3.7) the solution for u_1 is sought in the form

$$u_1 = \xi^{\alpha}\,u_{10}(\eta) + \ldots. \tag{3.12}$$

Then, from (3.11*a*), with coefficients given by (3.9)–(3.10), we have the equation

$$\tfrac{1}{2}\eta\,\mathrm{d}u_{10}/\mathrm{d}\eta - \{\alpha + [2c_0/(c_0+\eta^2)]\}\,u_{10} = 0 \tag{3.13}$$

for u_{10}, if, in addition, $\alpha < -1$ (non-uniform terms should be incorporated if $\alpha = -1$ in the right-hand side). The solution for (3.13) is

$$u_{10} = c_{10}\,\eta^{2\alpha+4}/(c_0+\eta^2)^2 \tag{3.14}$$

with an arbitrary constant c_{10}. The function u_{10} must be regular at finite η, however, which gives the spectrum of eigenvalues α as

$$\alpha = \tfrac{1}{2}(m-4), \quad m = 0, 1, \ldots. \tag{3.15}$$

PHILOSOPHICAL TRANSACTIONS OF THE ROYAL SOCIETY A MATHEMATICAL, PHYSICAL & ENGINEERING SCIENCES
PHILOSOPHICAL TRANSACTIONS OF THE ROYAL SOCIETY A MATHEMATICAL, PHYSICAL & ENGINEERING SCIENCES

Downloaded from rsta.royalsocietypublishing.org

The first eigenfunction should typically be chosen in the local solution, yielding the final result for the function u_1 in the inviscid region,

$$u_1 = \xi^{-2} u_{10}(\eta) + \ldots, \quad u_{10} = c_{10}(c_0 + \eta^2)^{-2}. \tag{3.16}$$

In a similar way the leading term of the solution for w_1 is determined from (3.11*b*) as

$$w_1 = \xi^{-4} w_{10}(\eta) + \ldots, \quad w_{10} = d_{10}(c_0 + \eta^2)^{-4}, \tag{3.17}$$

with an arbitrary coefficient d_{10}.

It follows from (3.9*b*), (3.17) that the original symmetry-plane expansion (3.3) is only valid in a region gradually narrowing in z, on approach to the singularity, defined by $z^2 \ll (-x)^3$, $x \to -0$. To obtain the solution in a complete 3-D neighbourhood of the singularity we consider the extension of the symmetry-plane inviscid layer (3.7) in the region $z = O(|x|^{\frac{3}{2}})$ and define new independent variables of order one, as $\xi = -x \to +0$,

$$\eta = (\psi - \psi_0)\,\xi^{-\frac{1}{2}}, \quad \zeta = z\xi^{-\frac{3}{2}}. \tag{3.18}$$

The solution for (3.2*a–c*) is now expanded, from (3.3), (3.9), (3.16), (3.17), as

$$u = U(\eta, \zeta) + \ldots, \quad w = \xi^{\frac{1}{2}} W(\eta, \zeta) + \ldots, \quad r = \xi^{-1} R(\eta, \zeta) + \ldots. \tag{3.19}$$

The equations for the leading terms in (3.19) are

$$\frac{\eta}{2a_{00}} U \frac{\partial U}{\partial \eta} + \left(\frac{3\zeta}{2a_{00}} U + \frac{W}{b_{00}} \right) \frac{\partial U}{\partial \zeta} = 0, \tag{3.20a}$$

$$\frac{\eta}{2a_{00}} U \frac{\partial W}{\partial \eta} + \left(\frac{3\zeta}{2a_{00}} U + \frac{W}{b_{00}} \right) \frac{\partial W}{\partial \zeta} - \frac{UW}{2a_{00}} = 0. \tag{3.20b}$$

$$\frac{1}{a_{00}} \left[UR + \tfrac{1}{2}\eta \frac{\partial (UR)}{\partial \eta} + \tfrac{3}{2}\zeta \frac{\partial (UR)}{\partial \zeta} \right] + \frac{1}{b_{00}} \frac{\partial (WR)}{\partial \zeta} = 0. \tag{3.20c}$$

Boundary conditions are formulated from matching requirements with the solution above, in the form

$$\text{as} \quad \zeta \to 0, \quad U \to \bar{u}_0, \quad W = -\zeta \frac{b_{00}\,\bar{u}_0\,c_0}{a_{00}(c_0 + \eta^2)} + \zeta^3 \frac{d_{10}}{(c_0 + \eta^2)^4} + O(\zeta^5), \tag{3.21a,b}$$

$$R \to c_0\, d_0 / [\bar{u}_0\, b_{00}(c_0 + \eta^2)]. \tag{3.21c}$$

It can be shown that the unique solution of (3.20*a*, *b*) with the boundary conditions (3.21*a*, *b*) is

$$U = \bar{u}_0 = \text{const.}, \tag{3.22a}$$

$$\gamma^4 d_{10}\, W^3 + 8\gamma c_0^3 (c_0 + \eta^2)\, W + 16 c_0^4 \zeta = 0. \tag{3.22b}$$

Here $\gamma = 2a_{00}/(\bar{u}_0\, b_{00})$ and an implicit representation for W is used. From (3.20*c*), (3.21*c*) the function $R(\eta, \zeta)$ is now determined as

$$R = 8c_0^4\, d_0\, \bar{u}_0^{-1}\, b_{00}^{-1} [3\gamma^3 d_{10}\, W^2 + 8c_0^3 (c_0 + \eta^2)]^{-1}, \tag{3.22c}$$

making use of (3.22*a*, *b*).

The solution above can be obtained from rather standard procedures applicable to the first-order quasi-linear equations (3.20*a–c*). The only unusual feature of the problem worth mentioning here is the particular form of the boundary conditions

PHILOSOPHICAL TRANSACTIONS OF THE ROYAL SOCIETY A MATHEMATICAL, PHYSICAL & ENGINEERING SCIENCES
PHILOSOPHICAL TRANSACTIONS OF THE ROYAL SOCIETY A MATHEMATICAL, PHYSICAL & ENGINEERING SCIENCES

Downloaded from rsta.royalsocietypublishing.org

(3.21a–c) providing the uniqueness of the solution. It follows from properties of the characteristics of (3.20) that two terms of the expansion must be prescribed for the function W as $\zeta \to 0$ (to incorporate in the solution (3.22b) two arbitrary constants c_0, d_{10}), while only the leading terms in U, R are necessary, to include in (3.22a, c) two more parameters $\bar{u}_0$, d_0.

Omitting details of the derivation of the solution, we can, however, substantiate the appearance of the final relations (3.22a–c) from a more general viewpoint, noticing that (3.20a–c) in fact describe one particular self-similar solution of the hyperbolic system of inviscid equations

$$\frac{u}{a_{00}}\frac{\partial u}{\partial x}+\frac{w}{a_{00}}\frac{\partial u}{\partial z}=0, \quad \frac{u}{a_{00}}\frac{\partial w}{\partial x}+\frac{w}{a_{00}}\frac{\partial w}{\partial z}=0, \tag{3.23a,b}$$

$$\frac{1}{a_{00}}\frac{\partial (ur)}{\partial x}+\frac{1}{b_{00}}\frac{\partial (wr)}{\partial z}=0. \tag{3.23c}$$

It is remarkable that the streamfunction ψ appears in (3.23) as a parameter. Equations (3.23a, b) are further simplified by introducing, instead of z, a new variable s, specifying particular streamlines at any streamsurface $\psi = \text{const.}$, so that $z = z(x, \psi, s)$ and

$$\partial z/\partial x = w(x, \psi, s)/u(x, \psi, s). \tag{3.24}$$

Here, without loss of generality, $a_{00} = b_{00} = 1$. In the new variables x, ψ, s equations (3.23a, b) are just

$$u\,\partial u/\partial x = 0, \quad u\,\partial w/\partial x = 0, \tag{3.25}$$

with the general solution being

$$u = u_0(\psi, s), \quad w = w_0(\psi, s) \tag{3.26}$$

and reflecting momentum conservation in an inviscid flow without pressure gradient. The equation of the streamlines (3.24) then gives

$$z = xw_0(\psi, s)/u_0(\psi, s)+z_0(\psi, s) \tag{3.27}$$

and, from the mass conservation in (3.23c), written in x, ψ, s variables as

$$\frac{\partial r}{\partial x} = -r\frac{\partial}{\partial s}\left(\frac{w_0}{u_0}\right)\Big/\left[x\frac{\partial}{\partial s}\left(\frac{w_0}{u_0}\right)+\frac{\partial z_0}{\partial s}\right], \tag{3.28}$$

we obtain an expression for r in the form

$$r(x, \psi, s) = r_0(\psi, s)\Big/\left[x\frac{\partial}{\partial s}\left(\frac{w_0}{u_0}\right)+\frac{\partial z_0}{\partial s}\right]. \tag{3.29}$$

Here $r_0(\psi, s)$ is, along with u_0, w_0, z_0, an arbitrary function of ψ, s.

In the local solution the leading terms of the expansions for the regular functions u_0, w_0, z_0, r_0 are taken near one particular streamline, say $s = 0$, $\psi = \psi_0$. We assume that the streamline chosen belongs to the symmetry plane $s = 0$ (which is also $z = 0$), and prescribe local symmetry of the solution with respect to $\psi = \psi_0$ as well as symmetry of u and antisymmetry of z, w to s, to obtain

$$\left.\begin{aligned} &u_0 = \bar{u}_0+\ldots, \quad w_0 = -\kappa_0 s+\ldots, \\ &z_0 = s[\kappa_1+\kappa_2(\psi-\psi_0)^2+\ldots]+s^3[\kappa_3+\ldots]+\ldots, r_0 = \kappa_4+\ldots \end{aligned}\right\} \tag{3.30}$$

Downloaded from rsta.royalsocietypublishing.org

as $s \to 0$, $\psi - \psi_0 \to 0$. Here $\bar{u}_0$, κ_i are all constants.

The solution appears to be singular if the leading coefficient κ_1 in the expansion for z_0 is zero. From (3.26), (3.27), (3.29), (3.30) we then have three relations

$$u = \bar{u}_0 + \dots, \tag{3.31a}$$

$$\frac{\kappa_3}{\kappa_0^3} w^3 + \left(\frac{\kappa_2}{\kappa_0}\psi^2 - \frac{x}{\bar{u}_0}\right) w - z + \dots = 0, \tag{3.31b}$$

$$r = \frac{\kappa_4}{\kappa_0}\left(\frac{3\kappa_3}{\kappa_0^3} w^2 + \frac{\kappa_2}{\kappa_0}\psi^2 - \frac{x}{\bar{u}_0}\right) + \dots, \tag{3.31c}$$

which are equivalent to the self-similar solution (3.19), (3.22*a–c*).

One might notice that the analysis of 3-D steady flows in terms of streamlines, although relevant to a different physical situation, is formally related to the Lagrangian description of finite-time singularities in unsteady boundary layers (Van Dommelen & Shen 1982; Van Dommelen & Cowley 1990), with hyperbolic properties of the locally inviscid boundary-layer equations being used in both cases.

We proceed now to the description of some features of the singularity given by the asymptotic solution (3.19), (3.22*a–c*). The expansion (3.19) is based on a small parameter $\xi = -x$, which was assumed positive. The solution is therefore valid in the region $x < 0$ only. We can, however, extend the solution into an even larger domain merely by rewriting the expansion in terms of a new small parameter. For instance, to derive a description valid for $z > 0$ we define

$$u = U^*(\eta^*, \zeta^*) + \dots, \quad w = z^{\frac{1}{3}} W^*(\eta^*, \zeta) + \dots, \tag{3.32a,b}$$

$$r = z^{-\frac{2}{3}} R^*(\eta^*, \zeta^*) + \dots, \quad z \to +0, \tag{3.32c}$$

where new independent variables are introduced by

$$\eta^* = (\psi - \psi_0) z^{-\frac{1}{3}} = O(1), \quad \zeta^* = x z^{-\frac{2}{3}} = O(1). \tag{3.33}$$

Then, from (3.22*a–c*), the expressions for the leading coefficients are

$$U^* = \bar{u}_0, \tag{3.34a}$$

$$\gamma^4 d_{10} W^{*3} + 8\gamma c_0^3 (\eta^{*2} - c_0 \zeta^*) W^* + 16 c_0^4 = 0, \tag{3.34b}$$

$$R^* = 8 c_0^4 d_0 \bar{u}_0^{-1} b_{00}^{-1} [3\gamma^3 d_{10} W^{*2} + 8 c_0^3 (\eta^{*2} - c_0 \zeta^*)]^{-1}. \tag{3.34c}$$

From the definition of $r(x, \psi, z)$ in (3.2*d*) and asymptotic properties of the solution (3.3*b, c*) as $\eta^* \to \pm\infty$, the leading term of the boundary-layer thickness $\delta(x, z)$ in the region $\zeta^* = O(1)$ is evaluated as

$$\delta = z^{-\frac{1}{3}} \delta_0(\zeta^*) + \dots \tag{3.35a}$$

with

$$\delta_0(\zeta^*) = \int_{-\infty}^{\infty} R^*(\eta^*, \zeta^*)\, \mathrm{d}\eta^*. \tag{3.35b}$$

The latter expression, after some routine manipulations, can be reduced to the elliptic integral

$$\delta_0 = K_0 \int_{\rho_0}^{+\infty} \frac{\mathrm{d}\rho}{(\rho^3 + \nu\rho^2 - \operatorname{sgn} d_{10})^{\frac{1}{3}}}, \tag{3.36}$$

where

$$\nu = (2c_0^4/\gamma|d_{10}|)^{\frac{1}{3}} \zeta^*, \quad K_0 = (c_0 d_0/\bar{u}_0 b_{00})\,(2c_0/\gamma|d_{10}|)^{\frac{1}{6}} \tag{3.37}$$

Downloaded from rsta.royalsocietypublishing.org

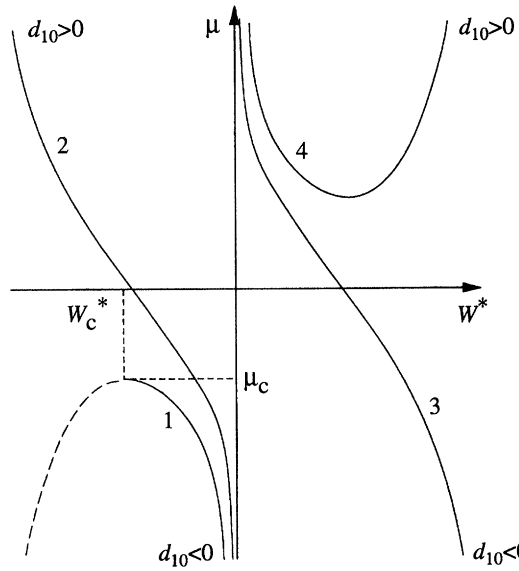

Figure 15. Qualitative behaviour of the function $\mu(W^*)$ defined by (3.40). Branches 1, 2 represent physically meaningful solutions; the first of them terminates at a singular point $\mu_c(W_c^*)$; the other is smooth in the entire interval $|\mu| < \infty$.

and $\rho_0(\nu)$ is the largest positive root of the equation

$$\rho_0^3 + \nu\rho_0^2 - \operatorname{sgn} d_{10} = 0. \tag{3.38}$$

The region of existence of the solution is now established from (3.34b), considering the combination

$$\mu = c_0\,\zeta^* - \eta^{*2} \tag{3.30}$$

as a function of W^*, namely

$$\mu = (\gamma^4 d_{10}\,W^{*3} + 16c_0^4)/(8\gamma c_0^3\,W^*). \tag{3.40}$$

As stated earlier, both γ, c_0 are positive. Then, depending on the sign of d_{10}, two different functions μ must be considered, as shown (qualitatively) in figure 15. Only branches 1 and 2 are relevant to our study because of the matching requirement with the symmetry-plane solution upstream of the singularity: $W^* \to 0$ as $\mu \to -\infty$. We therefore consider the two possibilities in turn below.

Case 1, d_{10} negative

As can be seen from figure 15, curve 1, the symmetry-plane solution $\mu \to -\infty$, $W^* \to -0$, can be continued up to the critical point

$$\mu_c = -\tfrac{3}{2}(\gamma|d_{10}|/c_0)^{\frac{1}{3}}, \quad W_c^* = -(2c_0/\gamma)\,(c_0/\gamma|d_{10}|)^{\frac{1}{3}}. \tag{3.41}$$

from (3.40). The dashed portion of curve 1 gives a physically meaningless solution.

Although the same value of $\mu = \mu_c$ predicts the appearance of the singularity at different ζ^*-stations for various stream surfaces $\eta^* = \text{const.}$, a crisis of the boundary layer first occurs at minimum ζ^*, which is $\zeta_c^* = -3(|d_{10}|\gamma/c_0)^{\frac{1}{3}}/(2c_0)$ and corresponds

Downloaded from rsta.royalsocietypublishing.org

to $\eta^* = 0$. Thus a regular solution for the 3-D BL equations exists in the domain $|z| < z_s(x)$, where

$$z_s(x) = (-x)^{\frac{3}{2}}(2c_0/3)^{\frac{3}{2}}(c_0/\gamma|d_{10}|)^{\frac{1}{2}} \tag{3.42}$$

at small $(-x)$.

The nature of the singularity can be established easily by considering the component of the velocity normal to the singular line (3.42). Defining $\zeta^* = \zeta_c^* + N$ with N measuring the distance to the singular line, the normal velocity is obtained from (3.32), (3.34*a*, *b*), (3.42) as

$$u_N = (4c_0/3\gamma)\,(c_0/\gamma|d_{10}|)^{\frac{2}{3}}(-c_0 x)^{\frac{1}{2}}(\eta^{*2} - c_0 N)^{\frac{1}{2}} + \ldots \tag{3.43}$$

with $N \to -0$ and $\eta^* = O(|N|^{\frac{1}{2}})$. The singularity therefore corresponds to a zero minimum in the velocity profile u_N, attained in the middle of the boundary layer. Essentially the same singular behaviour was studied earlier in the context of 2-D flow on a moving wall (Sychev 1980; Elliott *et al.* 1983). The quasi-2-D character of the solution (3.43) in fact follows from the momentum balances normal and tangential to the singular line. It is remarkable, however, that, in contrast with 2-D flows where the development of an internal singularity of this kind necessitates an adverse pressure gradient, the breakdown of the 3-D boundary layer may be due solely to the centrifugal forces in the x–z plane supported by the curvature of the singular line (3.42), i.e. it can occur with *favourable or adverse* pressure gradient.

In accordance with the quasi-2-D properties of the singularity, a logarithmic growth in the boundary-layer thickness of the form

$$\delta = (c_0 d_0/2\bar{u}_0 b_{00})\,(1/\sqrt{(-c_0 x)})\,[\ln(-N) + O(1)], \quad \text{as} \quad N \to -0, \tag{3.44}$$

is deduced either from (3.35)–(3.38) or from the known velocity field near the singular line.

Case 2, d_{10} positive

At curve 2, figure 15, both W^* and $\mathrm{d}\mu/\mathrm{d}W^*$ are negative (from (3.40)); then $W^*(\mu)$ is unique and regular on the μ-axis. This in turn leads to the conclusion, from (3.34*b*, *c*), that the solution for the original boundary-layer equations is regular in the entire 3-D neighbourhood of the singularity, excluding only the half-infinite portion of the symmetry plane $z = 0$, $x \gg 0$ (the downstream half). On approach to the symmetry plane at $x > 0$, however, we have that, as $z \to \pm 0$,

$$w = \mp(8c_0^3/\gamma^3 d_{10})^{\frac{1}{2}}[c_0 x - (\psi - \psi_0)^2]^{\frac{1}{2}} + \ldots \quad \text{if} \quad (\psi - \psi_0)^2 < c_0 x \tag{3.45a}$$

and

$$w \to 0 \quad \text{if} \quad (\psi - \psi_0)^2 > c_0 x, \tag{3.45b}$$

from (3.22*b*), (3.34*b*) and symmetry properties of the solution. From (3.45*a*) we conclude that a jump in the cross velocity or, in other words, a collision of boundary layers, occurs at the symmetry plane *downstream* of the singular point $x = 0$, the 'strength' of the collision being proportional to $x^{\frac{1}{2}}$. It is also interesting to note that the region of collision has quite definite boundaries $\psi - \psi_0 = \pm(c_0 x)$ and that the number of streamlines involved in the collision grows faster with distance from the origin $x = 0$.

One more fundamental feature of the discontinuous solution discussed above is the thickening of the boundary layer near the symmetry plane. As before, an appropriate estimate might be derived either from the general relations (3.35)–(3.38) or from evaluating the function $r = \partial y/\partial\psi$ (and then calculating the vertical coordinate y of the fluid particles in the limit $z \to 0$). In the latter case a more accurate analysis of the

PHILOSOPHICAL TRANSACTIONS OF THE ROYAL SOCIETY A MATHEMATICAL, PHYSICAL & ENGINEERING SCIENCES
PHILOSOPHICAL TRANSACTIONS OF THE ROYAL SOCIETY A MATHEMATICAL, PHYSICAL & ENGINEERING SCIENCES

Downloaded from rsta.royalsocietypublishing.org

cross velocity is necessary near the boundaries $\psi - \psi_0 = \pm (c_0 x)^{\frac{1}{2}}$, because the major contribution to the displacement effect at small $|z|$ happens to come from the thin layers $\psi - \psi_0 \mp (c_0 x)^{\frac{1}{2}} = O(|z|^{\frac{2}{3}} x^{-\frac{1}{2}})$. The final relation for the boundary-layer thickness in the vicinity of the symmetry plane is then

$$\delta(x,z) = \frac{c_0 d_0}{\bar{u}_0 b_{00}} \left\{ -\frac{\ln|z|}{\sqrt{(c_0 x)}} + \frac{3}{2}\frac{\ln(c_0 x)}{\sqrt{(c_0 x)}} + \frac{1}{\sqrt{(c_0 x)}} \left[\frac{1}{2} \ln \frac{c_0}{\gamma d_{10}} + \frac{7}{2} \ln 2 \right] + \ldots \right\}, \quad (3.46)$$

which is valid as $x \to +0$ (i.e. downstream of the symmetry-plane singularity), with $|z| \to 0$ and $|z| \ll x^{\frac{3}{2}}$.

4. Development of the discontinuity in the 3-D boundary layer

In this section we present results of a numerical solution of the original 3-D BL formulation (1.7*a–d*), (1.9*a–c*) for one particular case of the dent surface geometry. The solution seems to contain, as we intend to show, a discontinuity along the centreplane that starts from the inviscid internal breakdown of the smooth flow described above in §§2 and 3.

There are two major reasons for the numerical treatment of the full equations to be made in addition to our study of the symmetry-plane flow in §2 and the asymptotic analysis of the 3-D neighbourhood of singularity in §3. First, the description of the centre-plane flow was performed in Crocco variables, implying (quite arbitrarily) monotonicity of the streamwise velocity profile. An independent treatment based on cartesian coordinates therefore provides a necessary confirmation of the approach taken in §2. Second, only solution of the full initial-boundary-value problem can select one of the two singular forms suggested by the local study in §3, namely the one with a downstream discontinuity/collision or that with breakdown at some singular line.

The shape of the dent considered in this section is given by (1.10*a*, *b*). Owing to symmetry with respect to the plane $z = 0$ the computation domain is defined as $x \geqslant 0$, $y \geqslant 0$, $0 \leqslant z \leqslant b\sqrt{m}$. The value $m = 4$ was taken to provide a smooth entry solution at the leading and lateral boundaries $x = 0+$, $z = b\sqrt{m} - 0$ respectively. Also, the dent is assumed to be narrow, $b = 0.2$, but sufficiently deep, $h = -0.4$, to make the flow strongly 3-D and nonlinear. The corresponding symmetry-plane flow is described in §2*b*, i.e. the case $h = -0.4$, $h_w = h/b^2 = -10$, and some features of the solution are shown in figures 13, 14 and 16. According to our symmetry-plane calculations, the inviscid singularity in the middle of the BL develops at $x = x_s = 0.5934$. The value of the streamwise (crosswise) component of the pressure gradient is negative (positive) in the region $0 < x < x_0 = 0.6625$ (which contains the singular point), as follows from (1.7*d*), (1.10*a*, *b*). Hence the cross-flow velocity is directed towards the centreplane, at least near the boundaries $z = b\sqrt{m}$, $x = 0$, and the boundary conditions at $x = 0$, $0 \leqslant z \leqslant b\sqrt{m}$ and $x \geqslant 0$, $z = b\sqrt{m}$ can be formulated as

$$u = y, \quad w = 0. \quad (4.1)$$

The description of the numerical method is given in Appendix B. From the principle of zones of influence, the finite-difference approximation of z-derivatives in the momentum equations (1.7*a*, *b*) must be adjusted to the flow direction (which is found to be towards the plane $z = 0$ throughout the region $0 < x < x_0$). There exists, however, some possible freedom in the approximation of the term $\partial w/\partial z$ in the continuity equation (1.7*c*), and this question is also addressed below.

Downloaded from rsta.royalsocietypublishing.org

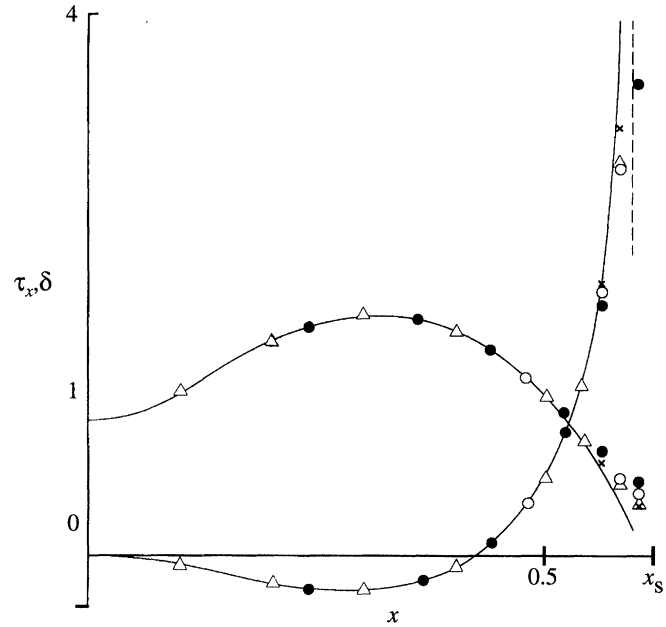

Figure 16. Streamwise skin friction $\tau_x(x, z=0)$ and displacement thickness $\delta(x, z=0)$ in the centreplane of the half-infinite dent (1.10) with $h=-0.4$, $b=0.2$, $m=4$. Comparison is made between the symmetry-plane calculations in Crocco variables in §2*b* (shown here with continuous lines) and numerical solution of the full 3-D BL equations in cartesian form, obtained with a uniform grid and the outward approximation (4.2), as described in §4. Grids used in the full 3-D calculations have: △, $[\Delta x, \Delta y, N_y, N_z] = [0.001, 0.025, 280, 121]$, ×, [0.001, 0.05, 280, 121]. ○, [0.002, 0.05, 280, 60], ●, [0.002, 0.05, 280, 30]. The vertical dashed line marks the position of the singularity, $x_s = 0.5934$.

For convenience we divide the calculations into three sets as follows. In the first series, computations were performed with a uniform grid in the z-direction and an approximation outward with respect to the centreplane approximation for $\partial w/\partial z$ in the continuity equation (1.7*d*), so that in effect

$$(\partial w/\partial z)\,(x, y, z) \approx [w(x, y, z+\Delta z) - w(x, y, z)]/\Delta z. \tag{4.2}$$

The results were tested with respect to the influence of the total numbers N_z, N_y of mesh points along the z-axis and y-axis respectively, and of the steplengths Δx, Δy.

Comparison of the calculated flow functions at $z=0$ with those obtained in the symmetry-plane study in §2*b* is shown in figure 16. We notice that the results are in a good agreement in the main portion of the flow $0 \leqslant x \leqslant 0.5$ even with only moderately small steps Δx, Δy and as little as 30 z-points. The trends in the solutions for $0.5 < x < x_s$, closer to the breakdown, seem to confirm the suggested locally inviscid scheme of the singularity, but quantitative comparison here is not completely satisfactory. The results in figure 16 suggest that the computational solution in the near-singularity region is highly sensitive to the values of Δz, Δx. Also, the refinement of the y-grid is not as essential here as the enlarging of the domain in the vertical direction, in view of the fast-growing displacement thickness.

In the second series of calculations the same outward approximation (4.2) as before

Downloaded from rsta.royalsocietypublishing.org

Figure 17

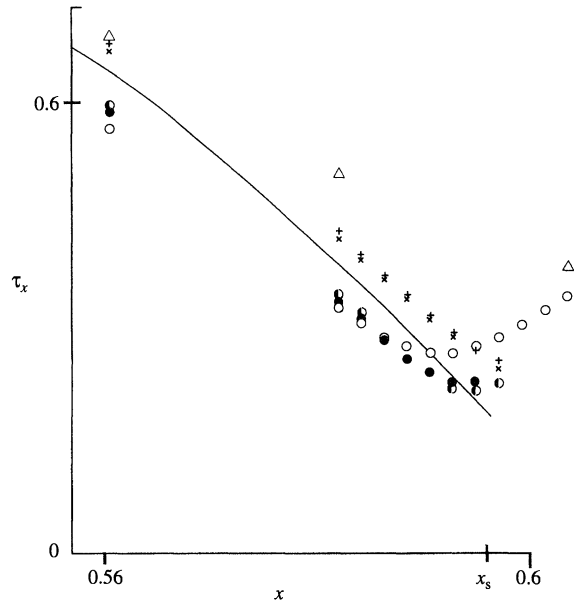

Figure 18

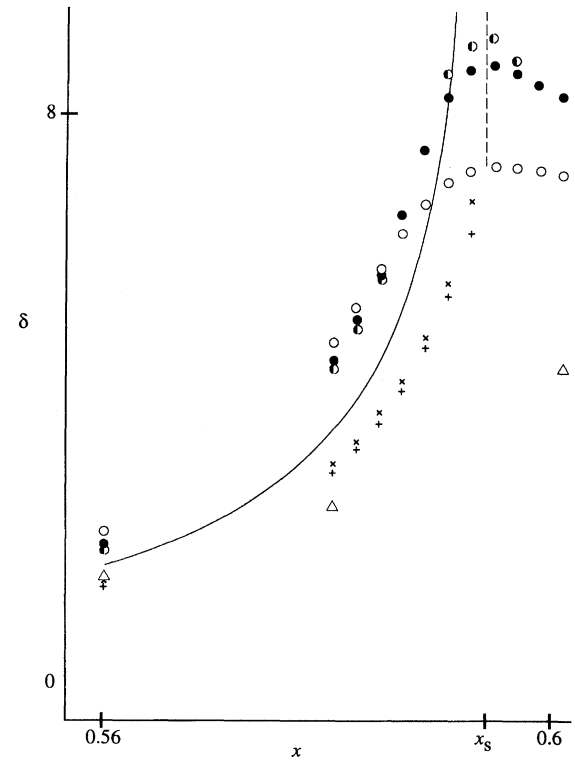

Figures 17 and 18. For description see opposite.

PHILOSOPHICAL TRANSACTIONS OF THE ROYAL SOCIETY A MATHEMATICAL, PHYSICAL & ENGINEERING SCIENCES

PHILOSOPHICAL TRANSACTIONS OF THE ROYAL SOCIETY A MATHEMATICAL, PHYSICAL & ENGINEERING SCIENCES

Downloaded from rsta.royalsocietypublishing.org

is used. But, in order to achieve higher resolution near the centreplane region without significant increase in the total number of z-points, an additional stretching of the lateral coordinate is included. So a new variable is defined as

$$\bar{z} = (a_1 z + a_2 z^2)/(a_3 + a_4 z) \tag{4.3}$$

with constants a_n such that the transformation remains regular, and mesh points are uniformly distributed along the $\bar{z}$-axis. In addition, the streamwise steplength Δx is taken about one tenth of the previous size to make it of the same order of magnitude as the smallest Δz-step. An immediate improvement of the computational description in the near-breakdown region is evident in figures 17 and 18, from comparing, for instance, the solutions obtained for uniform and stretched grids with equal numbers of points $N_z = 121$.

As concerns the flow beside the centreplane, the results obtained with the above two series are essentially close in the domain $0 \leqslant x < x_s$. Difficulties are, however, encountered in calculating the downstream portion of the BL at $x > x_s$. They stem basically from a breakdown of the finite-difference approximations in the region with a high level of displacement thickness. The loss of accuracy first occurs at small z near $x = x_s$ in the form of large-amplitude small-scale oscillations in the cross-velocity profile $w(y)$ near the upper boundary $y = y_{max}$. In the subsequent x-marching procedure, oscillations are transferred further outward from the centreplane, by means of the outward derivative (4.2), resulting in a damaged numerical solution within a wedge-like zone in the x–z plane downstream of $x = x_s$, $z = 0$.

Our main results were obtained in the third series of calculations, based again on the stretching (4.3). However, in contrast with the previous sets, an inward approximation of $\partial w/\partial z$ is used in (1.7*d*), defined by

$$(\partial w/\partial z)\,(x, y, z) \approx [w(x, y, z) - w(x, y, z - \Delta z)]/\Delta z] \tag{4.4}$$

effectively.

The influence of (4.4) on the symmetry-plane solution upstream of the singular point appears in figures 17 and 18 in higher values of the displacement thickness and smaller values of the skin friction. Up to $x \approx 0.588$ the error in reproducing the centreplane solution of §2*b* tends to be approximately of the same magnitude as in the second set but with opposite sign. The last feature seems to be in line with the first-order accuracy of the numerical method. Also, instead of the failure of solution encountered in the previous two sets, the displacement thickness now develops a strong maximum at the singular position, and can be continued downstream. This maximum in $\delta(x, z)$ grows, and presumably tends to infinity, with refinement of the steplength Δz, but to trace this process accurately and in full a further enlarging of the vertical scale of the calculation domain and diminishing of Δx are necessary.

General properties of the BL flow beside the centreplane are illustrated in figures

---

Figures 17 and 18. The flow functions in the symmetry plane of the half-infinite dent near the singular point: figure 17, streamwise skin friction; figure 18, displacement thickness. The results of the centreplane calculations of §2*b* are shown with continuous lines. Also shown are the results obtained in the three sets of calculations for the full 3-D BL equations: △, uniform z-grid and the outward approximation (4.2), the grid has $[\Delta x, \Delta y, N_y, N_z] = [0.001, 0.025, 280, 121]$; +, ×, stretched z-grid (4.3) and the outward approximation (4.2) with the grids [0.0002, 0.05, 280, 121], [0.0002, 0.05, 280, 201], respectively; ○, ●, ◐, the stretched grid and the inward approximation (4.4) with the grids [0.0002, 0.05, 280, 121], [0.0001, 0.05, 280, 201], [0.0001, 0.05, 280, 241], respectively.

PHILOSOPHICAL TRANSACTIONS OF THE ROYAL SOCIETY A MATHEMATICAL, PHYSICAL & ENGINEERING SCIENCES
PHILOSOPHICAL TRANSACTIONS OF THE ROYAL SOCIETY A MATHEMATICAL, PHYSICAL & ENGINEERING SCIENCES

Downloaded from rsta.royalsocietypublishing.org

Figure 19

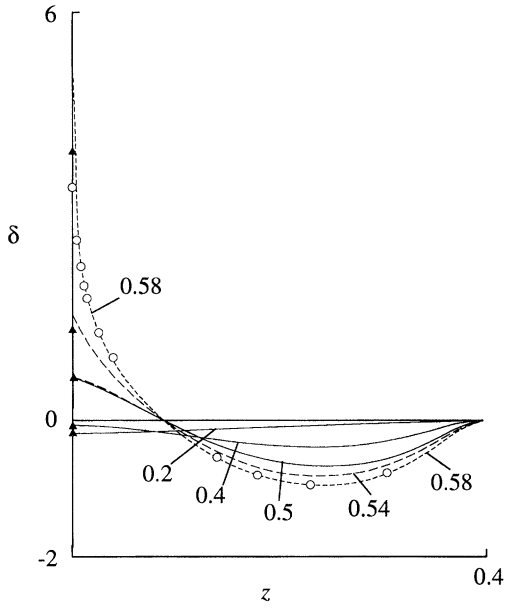

Figure 20

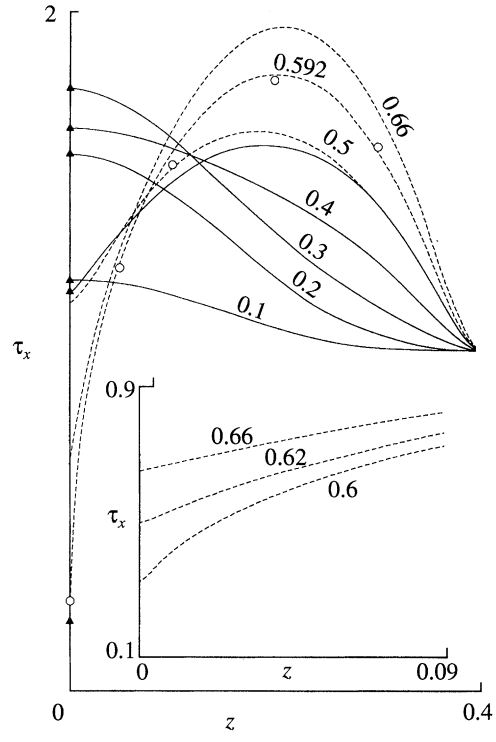

Figure 21

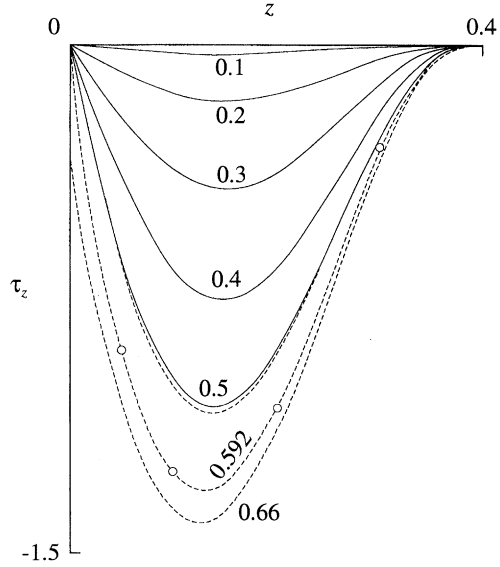

Figures 19–21. Spanwise distribution of the flow functions on the surface of the half-infinite dent at various x-sections: figure 19, displacement thickness $\delta(x,z)$; figure 20, streamwise skin friction $\tau_x(x,z)$; figure 21, crosswise skin friction $\tau_z(x,z)$. The x-positions are marked near the corresponding curves; —, the results in the region $0 < x \leqslant 0.5$ obtained in the first set of calculations in §4, the grid has $[\Delta x, \Delta y, N_y, N_z] = [0.001, 0.025, 280, 121]$; – – –, the results in the downstream portion $x \geqslant 0.5$ obtained in the third set of calculations, the grid has $[\Delta x, \Delta y, N_y, N_z] = [0.0001, 0.05, 280, 201]$. Comparison between the two calculations is made at $x = 0.5$. Also shown with ▲ are the symmetry-plane functions from §2b; ○, the results from the second set with the grid parameters [0.0002, 0.05, 280, 201]. The inset in figure 20 suggests the development of the finite slope in the streamwise skin friction distribution near the centreplane downstream of the breakdown of the smooth solution at $x = x_s = 0.5934$.

PHILOSOPHICAL TRANSACTIONS OF THE ROYAL SOCIETY A MATHEMATICAL, PHYSICAL & ENGINEERING SCIENCES
PHILOSOPHICAL TRANSACTIONS OF THE ROYAL SOCIETY A MATHEMATICAL, PHYSICAL & ENGINEERING SCIENCES

Downloaded from rsta.royalsocietypublishing.org

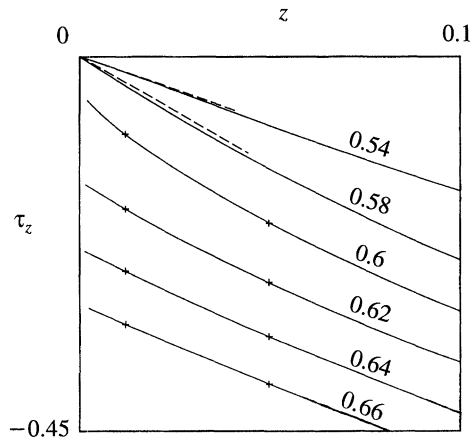

Figure 22. Near-centreplane behaviour of the crosswise skin friction $\tau_z(x, z)$ plotted against z, at various x-sections, suggesting the crossover from the regular solution at $x < x_s$ to one with the discontinuity/collision at $x > x_s$: —, the results of the full 3-D calculations in the third set of §4, the grid has $[\Delta x, \Delta y, N_y, N_z] = [0.0001, 0.05, 280, 201)$; + + +, the same grid as before but with $N_z = 241$; – – –, the limiting tangent at $z \to 0$ as calculated from the symmetry-plane equations in §2*b*.

19–21. Here the continuous curves represent the solution at $x \leqslant 0.5$ obtained with the uniform z-grid, and the dashed lines refer to the downstream flow at $x \geqslant 0.5$ calculated in the third series. The results from the two different sets can therefore be compared at $x = 0.5$ and they demonstrate good agreement in the displacement thickness $\delta(x, z)$ and in the crosswise skin friction $\tau_z = \partial w/\partial y$ $(y = 0)$ distributions. There is, however, some divergence in the prediction of the streamwise skin friction $\tau_x = \partial u/\partial y$ $(y = 0)$, with maximum relative deviation being of the order of 3%.

The major 3-D effect in this configuration appears in the strong deceleration of the near-centreplane flow, starting at $x \approx 0.3$ and continuing up to the breakdown at $x = x_s$, regardless of the favourable streamwise pressure gradient (figures 16 and 20). This is accompanied by the simultaneous growth of the BL thickness with its pronounced maximum at the centreline in figure 19. The spanwise extent of the deceleration region is roughly estimated, from the position of the maximum in τ_x and minimum in δ, as $0 \leqslant z \leqslant 0.2$ (see figures 19 and 20).

In spite of the breakdown of the smooth solution at $x = x_s$, $z = 0$, the calculations can be continued downstream of x_s at $z > 0$, and remain valid there, owing to the negative values of the cross-velocity in the entire BL. We usually terminated computations at $x = 0.66$ in fact, where the new structure of the flow field arising from the breakdown can already be seen in the numerical solution. For instance, finite limiting values of the lateral skin friction at $z \to 0$ indicate the development of the discontinuity along the symmetry plane at $x > x_s$, similar to, for instance, Howarth (1951), Stewartson *et al.* (1980) and Timoshin (1991). This property is illustrated in figure 21 and in more detail in figure 22. The dashed lines in figure 22 are shown for an additional comparison of the symmetry-plane solution in §2*b* with that obtained in the full 3-D formulation.

Another feature typical of BL collisions is in the finite slope of the streamwise skin friction τ_x at $z \to 0$, when compared with the regular symmetrical behaviour upstream of the singularity; compare the solutions at $x = 0.1$–0.5 and $x = 0.66$ in figure 20.

PHILOSOPHICAL TRANSACTIONS OF THE ROYAL SOCIETY A MATHEMATICAL, PHYSICAL & ENGINEERING SCIENCES
PHILOSOPHICAL TRANSACTIONS OF THE ROYAL SOCIETY A MATHEMATICAL, PHYSICAL & ENGINEERING SCIENCES

Downloaded from rsta.royalsocietypublishing.org

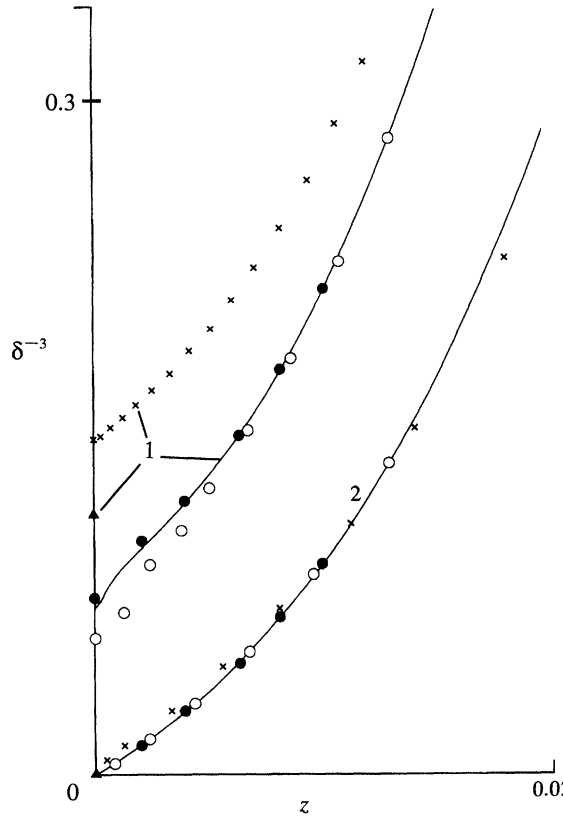

Figure 23. The function $\delta(x,z)^{-3}$ plotted against z at two x-sections is shown for the comparison between the numerical solution of the 3-D BL equations and the local theory in §3; 1, $x = 0.56$; 2, $x = 0.592$. The symmetry-plane results of §2b are marked with ▲; ×, the second set of the full 3-D calculations in §4 with the grid $[\Delta x, \Delta y, N_y, N_z] = [0.0002, 0.05, 280, 201]$. The other results are obtained in the third set: —, with the grid [0.0001, 0.05, 280, 201]; ○, [0.0002, 0.05, 280, 121]; ●, [0.0001, 0.05, 280, 241].

Hence, in accordance with the analytical predictions in §3, the inviscid symmetry-plane singularity gives rise to a BL collision downstream. Quantitative comparison between the theory and computations, based on the skin-friction study, seems to be difficult in our case, however, for the skin-friction development is contained in higher approximations in the local theory. Instead, we consider the distribution of the BL thickness near the singular point $x = x_s$, $z = 0$. As follows from the asymptotic relation (3.35a), the function $\chi(x,z) = \delta^{-3}(x,z)$ has a finite slope in z at the critical station $x = x_s$ so that

$$\chi(x,z) = z\delta_0(0)^{-3} + \ldots \quad \text{as} \quad z \to 0, \quad x = x_s, \tag{4.5}$$

and $\delta_0(0)$ is a positive constant. The computed function χ is depicted in figure 23 at the two successive cross-sections $x = 0.56$, $x = 0.592$. The first of them is far ahead of the breakdown, and so the minimum value of χ is non-zero. However, in the second section, which is much closer to the singularity, a linear portion of the graph appears clearly at small z. It is remarkable that the numerical results from different sets predict almost the same curve at $x = 0.592$ (very near $x = x_s$), whereas the difference

Downloaded from rsta.royalsocietypublishing.org

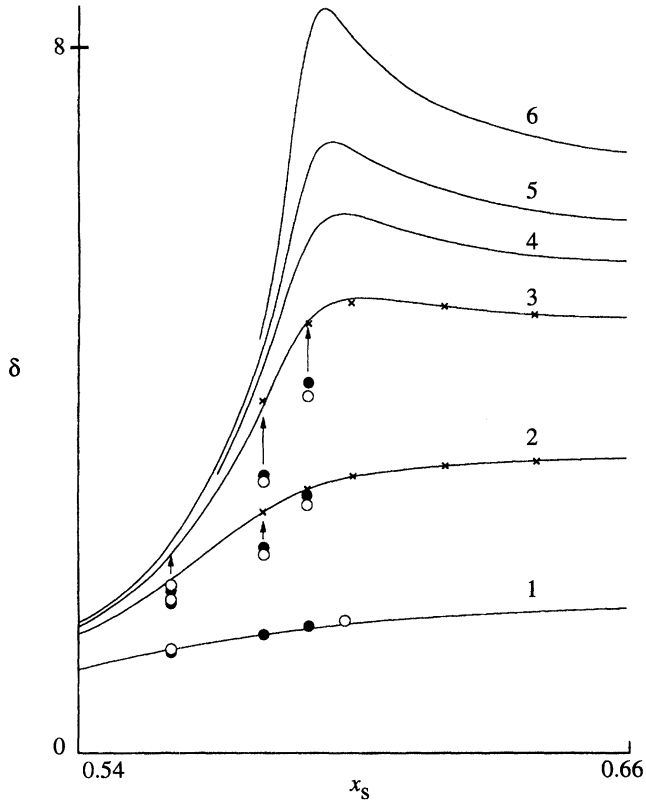

Figure 24. Distribution of the displacement thickness $\delta(x,z)$ plotted against x at various values of z in the 3-D neighbourhood of the singular point $x = x_s = 0.5934$, $z = 0$. Curves 1–6 refer to $z = 2.24\times10^{-2}$, 5.025×10^{-3}, 1.225×10^{-3}, 6.81×10^{-4}, 4.36×10^{-4}, 2.09×10^{-4}, respectively; —, numerical results from the third set with the grid $[\Delta x, \Delta y, N_y, N_z] = [0.0001, 0.05, 280, 201]$; ×, the results from the third set with grid [0.0002, 0.05, 280, 121]. Also shown are the results from the second set: ○, with the grid [0.0002, 0.05, 280, 201]; ●, the same grid but with $N_z = 121$.

in the data upstream is quite pronounced. This property seems to be due to the particular nature of the displacement effect in the flow considered, as explained in §3, because the main contribution to the BL thickness near the breakdown comes from the locally inviscid zone in the middle of the flow. This zone is likely to be captured well in our calculations referred to in figure 23. Another contribution, from the upper portion of the flow above the inviscid one, can be reproduced only with further enlarging of the y-scale of the computation domain. Inaccuracy in evaluation of the latter term is presumably suppressed by the strong growth of the main contribution as $x \to x_s$, but leads to some scattering of the results upstream.

Downstream of breakdown, the theory of §3 predicts a logarithmic expansion of the colliding layers as $z \to 0$, from (3.46). A precise proof of this logarithmic law could hardly be derived from numerical data, first on account of the inevitable numerical inaccuracy in the solution and secondly because of the significant influence of the next terms in the local relation (3.46). Nevertheless, the trend itself, i.e. the growth of the BL thickness near the centreplane, can be seen in figure 24, and that seems to

Downloaded from rsta.royalsocietypublishing.org

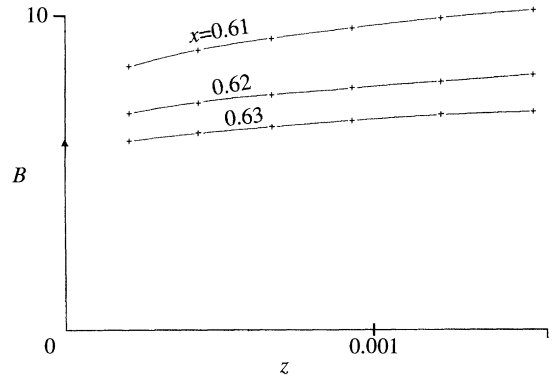

Figure 25. Comparison between the results of the numerical solution of the full 3-D BL equations and the analytic predictions in §3. The function $B(x,z)$ defined by (4.6) plotted against z, at various x: +, numerical results obtained in §4 in the third set of calculations with the grid $[\Delta x, \Delta y, N_y, N_z] = [0.0001, 0.05, 280, 201]$; ▲, the limiting value B_0 calculated from the symmetry-plane solution in §2b according to (4.8).

have the qualitative background of the theory. Further, an attempt at a quantitative estimate is shown in figure 25. According to (3.46), the function $B(x,z)$, defined as

$$B(x,z) = -\ln|z|/[\delta(x,z)\sqrt{(x-x_s)}], \tag{4.6}$$

should have a finite limit, $B(x,z) \to B_0$, as $x - x_s \to +0$, $z \to \pm 0$ and $|z| \ll (x-x_s)^{\frac{3}{2}}$. The limiting value of B_0 is a constant,

$$B_0 = \bar{u}_0 b_{00}/(c_0^{\frac{1}{2}} d_0), \tag{4.7}$$

which remains arbitrary in the local theory.

The crosses in figure 25 represent values of $B(x,z)$ obtained from our numerical solution by making use of (4.6). On the other hand, from the theory of §3, an independent estimate for the constant in (4.6), (4.7) can be deduced from the symmetry-plane solution ahead of the singularity, because the displacement-thickness growth, on approach to breakdown, obeys the local relation

$$\delta = (\pi/B_0)(-x)^{-\frac{1}{2}} + \ldots, \tag{4.8}$$

from (3.2d), (3.7), (3.9c), (3.10d). Thus from the symmetry-plane calculations in §2b we derive an estimate $B_0 = 6.3$. As is shown in figure 25, this turns out to be at least in order-of-magnitude agreement with the results of the full 3-D BL calculations.

5. Discussion

A number of suggestions and further questions stem from our study, we believe. We first address the structure of fully developed BL collision at a finite distance from the breakdown of smooth solutions. It is convenient to treat the flow behaviour in

Downloaded from rsta.royalsocietypublishing.org

Mises variables, assuming that the streamfunction can be properly defined at least locally near the centreplane. Then, as follows from the analysis in §3, the cross-velocity profile near the symmetry plane contains a portion of non-zero limiting values, such that as $z \to \pm 0$, for $x > x_s$,

$$w(x, \psi, z) = \mp w_0(x, \psi) + \ldots \quad \text{if} \quad \psi_1(x) < \psi < \psi_2(x), \tag{5.1}$$

where $\psi_{1,2}(x)$ define the boundaries of the region of collision. Above and below the collision region the cross-flow remains predominantly regular, leading to a usual centreplane expression of the form

$$w(x, \psi, z) = zW_0(x, \psi) + \ldots \quad \text{if} \quad \psi < \psi_1(x) \quad \text{or} \quad \psi > \psi_2(x). \tag{5.2}$$

The growth of the BL thickness appears as $z \to 0$ from the compression of fluid particles near the boundaries $\psi_{1,2}(x)$. One may suggest from analysis of the crosswise skin-friction distribution, in figures 21 and 22, that the lower boundary of the collision domain reaches the solid surface ($y = 0$) at some distance from the singularity in the symmetry-plane solution, resulting in an intersection of surface streamlines at $x > x_1 > x_s$, say. The position of such a 'surface streamlines' breakdown remains unknown within the framework of this paper, as well as the precise structure of the corresponding near-wall solution. It is also unclear whether the upper boundary $\psi = \psi_2(x)$ always remains in the middle of the flow or can be shifted towards the outer edge of the boundary layer at some other point $x = x_2 > x_s$. If both values of $x_{1,2}$ are finite, the colliding flows further downstream will have finite displacement thickness along the symmetry line.

A theory of the origin of discontinuity based on an assumption of bounded BL thickness everywhere except at the very first singular point was proposed in Stewartson *et al.* (1980). We argue, however, that this is unlikely to be the case in their particular problem (or others), because the breakdown of the smooth solution is initially related to a collision of near-wall fluid particles, according to SS, CSB. Hence even if the lower boundary of the colliding layer $\psi_1(x)$ coincides with the solid wall downstream of x_s, i.e. $x_1 = x_s$, the upper boundary $\psi_2(x)$ should be located in the middle of the flow, at least along some finite segment of the downstream x-axis. The latter implies the same as in §3, i.e. logarithmic thickening of the near-centreline layers.

Although the inviscid internal breakdown has been identified in §2 as the most typical one, taking into account its structural stability to variation of the local/global conditions, alternative routes for discontinuity development can presumably be obtained in more special cases, starting for example from the blow-up singularities studied in §2 or with those described in Smith & Walton (1989) and Walton & Smith (1992). Also, the effects of non-symmetry, compressibility, turbulence modelling, upstream/downstream moving walls and unsteadiness can provoke a variety of singularities in a 3-D BL flow.

Finally here, unbounded thickening of the BL along the discontinuity inevitably implies viscous–inviscid interaction affecting the flow field in a narrow neighbourhood of the centreline, most probably with the further prospect of the origin of an open-type separation. Another type of BL breakdown predicted in §3, with blow-up in the middle of the flow due to strong centrifugal forces, also deserves attention in view of an intriguing possibility of *internal* separation in steady 3-D flows, similar to 2-D steady separation on a moving wall and 2-D or 3-D unsteady separation.

Downloaded from rsta.royalsocietypublishing.org

However, detailed analysis of interaction/separation is beyond the scope of the present paper.

We should recap that overall the theory and computations in §§2–4 seem to be in broad agreement on the 3-D BL flow properties. They tend to confirm the frequent occurrence, and structural stability, of the singularity of internal mid-flow form in cases of favourable or zero pressure gradient, with the Goldstein singularity remaining the most likely outcome under an adverse gradient. The combination of analytical and numerical work appears to be very helpful in shedding extra light on the 3-D flow response. It is felt that more such studies should be made because 3-D BLs are clearly of importance in reality, whether in an interactive or non-interactive setting. Not least in this context is the application to BL transition, for example in describing the lift-off of lambda vortices, as discussed in §1.

Support from United Technologies, through Dr M. J. Werle, for S.N.T. and F.T.S., and from the Royal Society, for S.N.T., is gratefully acknowledged, as are computational facilities through SERC, including ULCC access.

Appendix A. Numerical method for the symmetry-plane equation

For the purpose of numerical treatment the symmetry-plane boundary-value problem was further transformed by introducing new variables

$$\phi(\xi,\eta)=\Omega^2, \quad W(\xi,\eta)=w_0/F(\eta), \tag{A 1}$$

where

$$F(\eta)=(1+c^2\eta^2)^{-\frac{1}{2}} \tag{A 2}$$

and the constant c was chosen as $c=\frac{1}{2}$.

The boundary-value formulation (2.4)–(2.7) is then

$$\eta\frac{\partial\phi}{\partial\xi}-2\phi WF-\frac{\mathrm{d}p_0}{\mathrm{d}\xi}\frac{\partial\phi}{\partial\eta}=\phi\frac{\partial^2\phi}{\partial\eta^2}-\frac{1}{2}\left(\frac{\partial\phi}{\partial\eta}\right)^2, \tag{A 3a}$$

$$\eta F\frac{\partial W}{\partial\xi}+F^2W^2-\frac{\mathrm{d}p_0}{\mathrm{d}\xi}\left(F\frac{\partial W}{\partial\eta}+\frac{\mathrm{d}F}{\mathrm{d}\eta}W\right)+2p_1=\phi F\frac{\partial^2W}{\partial\eta^2}+2\phi\frac{\mathrm{d}F}{\mathrm{d}\eta}\frac{\partial W}{\partial\eta}+\phi\frac{\mathrm{d}^2F}{\mathrm{d}\eta^2}W, \tag{A 3b}$$

$$\partial y/\partial\eta=\phi^{-\frac{1}{2}}, \tag{A 3c}$$

$$\text{at} \quad \xi=0, \quad \phi=1, \quad W=0, \tag{A 3d}$$

$$\text{at} \quad \eta=0, \quad \partial\phi/\partial\eta=2\,\mathrm{d}p_0/\mathrm{d}\xi, \quad W=y=0, \tag{A 3e}$$

$$\text{as} \quad \eta\to+\infty, \quad \phi\to1, \quad W\to-2c\int_0^\xi p_1(s)\,\mathrm{d}s, \quad y-\eta\to\delta_0(\xi). \tag{A 3f}$$

Thus, in the variables ϕ, W the nonlinearity in the wall boundary condition (2.5a) is removed. Also, instead of the trivial condition for w_0 at the outer edge of the boundary layer (2.5b), the leading term of the asymptotic solution as $\eta\to+\infty$ is incorporated in (A 3f).

A finite-difference approximation of (A 3a, b) second-order accurate in both ξ, η was used, with constant step $\Delta\eta$ and variable step in ξ (although the variable

Downloaded from rsta.royalsocietypublishing.org

ξ-step was used in test calculations only to clarify the particular type of singularity encountered). With $(\phi^1_\kappa, W^1_\kappa)$, $(\phi^2_\kappa, W^2_\kappa)$ being known functions at $(\xi = \xi_1, \eta = (\kappa-1)\,\Delta\eta)$, $(\xi = \xi_2, \eta = (\kappa-1)\,\Delta\eta)$ respectively and $\xi_2 = \xi_1 + d_1$, the solution at the next step $\xi_3 = \xi_2 + d_2$ was evaluated from the equations

$$\phi^n_{\kappa+1}\left(8\phi^3_\kappa - \phi^3_{\kappa+1} + \phi^3_{\kappa-1} + 4\Delta\eta\,\frac{\mathrm{d}p_0}{\mathrm{d}\xi}(\xi_3)\right) + \phi^n_\kappa(-16\phi^3_\kappa - 8(\Delta\eta)^2\frac{d_3}{d_5}\eta_\kappa + 16(\Delta\eta)^2 F_\kappa W^3_\kappa)$$

$$+\,\phi^n_{\kappa-1}\left(8\phi^3_\kappa + \phi^3_{\kappa+1} - \phi^3_{\kappa-1} - 4\Delta\eta\,\frac{\mathrm{d}p_0}{\mathrm{d}\xi}(\xi_3)\right) = \frac{8(\Delta\eta)^2}{d_5}\eta_\kappa(d_2^2\,\phi^1_\kappa - d_4\,\phi^2_\kappa), \quad (\mathrm{A}\,4a)$$

$$W^n_{\kappa+1}\left(F_\kappa\phi^3_\kappa + \Delta\eta\,\phi^3_\kappa\left(\frac{\mathrm{d}F}{\mathrm{d}\eta}\right)_\kappa + \tfrac{1}{2}\Delta\eta\,\frac{\mathrm{d}p_0}{\mathrm{d}\xi}(\xi_3)\,F_\kappa\right)$$

$$+\,W^n_\kappa\left(-2F_\kappa\phi^3_\kappa + (\Delta\eta)^2\phi^3_\kappa\left(\frac{\mathrm{d}^2F}{\mathrm{d}\eta^2}\right)_\kappa - (\Delta\eta)^2\frac{d_3}{d_5}\eta_\kappa F_\kappa - (\Delta\eta)^2\,W^3_\kappa(F_\kappa)^2\right.$$

$$\left.+\,(\Delta\eta)^2\frac{\mathrm{d}p_0}{\mathrm{d}\xi}(\xi_3)\left(\frac{\mathrm{d}F}{\mathrm{d}\eta}\right)_\kappa\right) + W^n_{\kappa-1}\left(F_\kappa\phi^3_\kappa - \Delta\eta\phi^3_\kappa\left(\frac{\mathrm{d}F}{\mathrm{d}\eta}\right)_\kappa - \tfrac{1}{2}\Delta\eta\,\frac{\mathrm{d}p_0}{\mathrm{d}\xi}(\xi_3)\,F_\kappa\right)$$

$$= (\Delta\eta)^2\left(2p_1(\xi_3) + \frac{\eta_\kappa F_\kappa}{d_5}(d_2^2\,W^1_\kappa - d_4\,W^2_\kappa)\right), \quad (\mathrm{A}\,4b)$$

$$d_3 = d_1^2 + 2d_1\,d_2, \quad d_4 = (d_1+d_2)^2, \quad d_5 = d_1\,d_2(d_1+d_2). \quad (\mathrm{A}\,4c)$$

Here a simple iterative procedure was applied to handle the nonlinearity in the equations. The coefficients in the nonlinear derivatives at $\xi = \xi_3$ were calculated based on the solution $(\phi^3_\kappa, W^3_\kappa)$ from the previous iteration, therefore leading to linear equations for $(\phi^n_\kappa, W^n_\kappa)$ at the next iteration.

Equation (A 3*c*) was approximated as

$$y_{\kappa+1} - y_\kappa = \tfrac{1}{2}\Delta\eta\,((\phi^n_{\kappa+1})^{-\frac{1}{2}} + (\phi^n_\kappa)^{-\frac{1}{2}}), \quad (\mathrm{A}\,4d)$$

and a three-point approximation of the first derivative in η was used to evaluate the crosswise skin friction

$$\tau_z = \tau_x\,\partial(WF)/\partial\eta \quad (\eta = 0), \quad (\mathrm{A}\,5)$$

while the streamwise skin friction is just $\tau_x = (\phi^n_1)^{\frac{1}{2}}$.

The numerical method above was found to be quite efficient in regions where the solution is smooth. The number of iterations necessary to provide a solution with accuracy $\Sigma_\kappa[(\phi^3_\kappa - \phi^n_\kappa)^2 + (W^3_\kappa - W^n_\kappa)^2] \leqslant 10^{-6}$ was typically 3–5 for the regular solution but increasing to 15–20 on approach to the singularity. Further details of the grids used are given in the legends to corresponding figures.

Appendix B. Numerical method for the full 3-D BL

A relatively simple and straightforward method was used for the full 3-D BL, governed by the three equations (1.7*a*–*c*) with pressure (1.7*d*), boundary conditions (1.9*a*–*c*) and hump shape (1.10*a*, *b*). The approach is an explicit one extending an

Downloaded from rsta.royalsocietypublishing.org

approach for 2-D flows developed by the late Professor R. T. Davis (private communications, 1982–1984). Thus the three equations are discretized as

$$\bar{u}_{jk}(u_{jk}-\bar{u}_{jk})/(\Delta x)+v_{jk}(\bar{u}_{j+1m}-\bar{u}_{j-1m})/(2\Delta y)+\bar{w}_{jk}[dr(u_{jk}-u_{jk-1}) + (1-dr)(u_{jk+1}-u_{jk})]/(\Delta z)+px=(u_{j+1k}-2u_{jk}+u_{j-1k})/(\Delta y)^2, \quad (B\,1)$$

$$\bar{u}_{jk}(w_{jk}-\bar{w}_{jk})/(\Delta x)+v_{jk}(\bar{w}_{j+1k}-\bar{w}_{j-1k})/(2\Delta y)+\bar{w}_{jk}[dr(w_{jk}-w_{jk-1}) + (1-dr)(w_{jk+1}-w_{jk})]/(\Delta z)+pz=(w_{j+1k}-2w_{jk}+w_{j-1k})/(\Delta y)^2, \quad (B\,2)$$

$$(u_{jk}+u_{j-1k}-\bar{u}_{jk}-\bar{u}_{j-1k})/(2\Delta x)+(v_{jk}-v_{j-1k})/(\Delta y)+[dr(w_{jk}+w_{j-1k} - w_{jk-1}-w_{j-1k-1})+(1-dr)(w_{jk+1}+w_{j-1k-1}-w_{jk}-w_{j-1k})]/(2\Delta z)=0. \quad (B\,3)$$

where the overbars refer to known velocity values at the station x_{i-1} previous to the current calculation station $x_i=(i-1)\Delta x$. Here Δx, Δy, Δz are the suitably small step sizes in x, $y=(j-1)\Delta y$, $z=(k-1)\Delta z$, the subscripts j, k refer to function values at y, z nodes respectively, and the direction coefficient $dr=1$, 0 depending on whether $\bar{w}_{jk}$ is positive or negative. In the motions of present concern dr is mostly zero (see §4), which simplifies the computations, for example regarding the sweeping direction in z, although as is also discussed in §4, dr was replaced by unity in (B 3) for some runs.

The finite-difference equations (B 1), (B 2), for $j=2$ to $J-1$, and (B 3) for $j=2$ to J, are combined with the appropriate discrete versions of the boundary conditions on $\{u_1, v_1, w_1, (u_J-u_{J-1}), w_J\}_k$, where $(J-1)\Delta y$ denotes the suitably large outer boundary chosen, to yield $(u, v, w)_{jk}$ for all j by a single matrix inversion, at each k, covering the required z range in the k-decreasing direction if dr is zero as above. Then the procedure is moved on to the next x station. The starting conditions, at $x=0$, $i=1$, are inserted analytically, and likewise for px, pz in (B.1), (B.2), modelling $\partial p/\partial x$, $\partial p/\partial z$, which are evaluated analytically at the i, k location in x, z. The scheme above is only first-order accurate in x, z, owing mainly to the decision to linearize the inertia terms for the sake of simplicity. Earlier tests on 2-D and 3-D flow calculations suggest, however, that the scheme works well and accurately even for not excessively small step sizes. We note in passing the attractive alternative of using (B 1) to determine u_{jk} directly, then (B 2) for w_{jk}, then (B 3) for v_{jk}, if the $v\partial/\partial y$ terms are discretized differently. Stretching in z was also introduced readily, as described in §4, where the computational results are presented.

References

Blasius, H. 1908 Grenzschichten in Flüssigkeiten mit kleiner Reibung. *Z. Math. Phys.* **56**(1), 1–37.

Brown, S. N. 1965 Singularities associated with separating boundary layers. *Phil. Trans. R. Soc. Lond.* A **257**, 409–444.

Brown, S. N. 1985 Marginal separation of a three-dimensional boundary layer on a line of symmetry. *J. Fluid Mech.* **158**, 95–111.

Brown, S. N., Cheng, H. K. & Smith, F. T. 1988 Nonlinear instability and break-up of separated flows. *J. Fluid Mech.* **193**, 191–216.

Brown, S. N. & Simpson, C. J. 1982 Collision phenomena in free-convective flow over a sphere. *J. Fluid Mech.* **124**, 123–138.

Brown, S. N. & Stewartson, K. 1983 On an integral equation of marginal separation, *SIAM J. appl. Math.* **43**(5), 1119–1126.

Buckmaster, J. 1972 Perturbation technique for the study of three-dimensional separation. *Phys. Fluids* **15**(12), 2106–2113.

PHILOSOPHICAL TRANSACTIONS OF THE ROYAL SOCIETY A MATHEMATICAL, PHYSICAL & ENGINEERING SCIENCES

PHILOSOPHICAL TRANSACTIONS OF THE ROYAL SOCIETY A MATHEMATICAL, PHYSICAL & ENGINEERING SCIENCES

Downloaded from rsta.royalsocietypublishing.org

Cebeci, T., Khattab, A. K. & Stewartson, K. 1980 On nose separation. *J. Fluid Mech.* **97**, 435–454.

Cebeci, T., Khattab, A. K. & Stewartson, K. 1981 Three-dimensional laminar boundary layers and the ok of accessibility. *J. Fluid Mech.* **107**, 57–87.

Cebeci, T., Stewartson, K. & Brown, S. N. 1983 Nonsimilar boundary layers on the lesside of cones at incidence. *Int. J. Comput. Fluids* **11**(3), 175–186.

Cousteix, J. & Houdeville, R. 1981 Singularities in three-dimensional turbulent boundary-layer calculations and separation phenomena. *AIAA J* **19**(8), 976–985.

Cowley, S. J., Van Dommelen, L. L. & Lam, S. T. 1990 On the use of lagrangian variables in descriptions of unsteady boundary-layer separation. *Phil. Trans. R. Soc. Lond.* A **333**, 343–378.

Crabtree, L. F., Küchemann, D. & Sowerby, L. 1963 In *Laminar boundary layers* (ed. L. Rosenhead), chapter 8. Oxford University Press.

Davis, R. T. & Werle, M. J. 1982 Progress on interacting boundary layer computations at high Reynolds number. in *Numerical and physical aspects of aerodynamic flows* (ed. T. Cebeci). Springer-Verlag.

Dennis, S. C. R. & Chang, G.-Z. 1969 Numerical integration of the Navier–Stokes equations for steady two-dimensional flow. *Phys. Fluids* **12**(12), 88–93.

Duck, P. W. 1989 Three-dimensional marginal separation. *J. Fluid Mech.* **202**, 559–575.

Edwards, D. E. 1987 Analysis of three-dimensional separated flow using interacting boundary-layer theory. In *Boundary-layer separation*, pp. 163–178. Springer-Verlag.

Elliott, J. W. & Smith, F. T. 1987 Dynamic stall due to unsteady marginal separation. *J. Fluid Mech.* **179**, 489–512.

Elliott, J. W., Smith, F. T. & Cowley, S. J. 1983 Breakdown of boundary layers: (i) on moving surfaces; (ii) in semi-similar unsteady flow; (iii) in fully unsteady flow. *Geophys. Astrophys. Fluid Dyn.* **25**, 77–138.

Goldstein, S. 1948 On laminar boundary-layer flow near a position of separation. *Q. Jl Mech. appl. Math.* **1**, 43–69.

Howarth, L. 1951 Note on the boundary layer on a rotating sphere. *Phil. Mag.* **42**, 1308–1315.

Kachanov, Y. S., Ryzhov, O. S. & Smith, F. T. 1993 Formation of solitons in transitional boundary layers: theory and experiment. *J. Fluid Mech.* **251**, 273–297.

Kerimbekov, R. M., Ruban, A. I. & Walker, J. D. A. 1994 Hypersonic boundary-layer separation on a cold wall. *J. Fluid Mech.* **274**, 163–195.

Lighthill, M. J. 1963 In *Laminar boundary layers* (ed. L. Rosenhead), chapter 2. Oxford University Press.

Lipatov, I. I. 1980 Weakly interactive hypersonic boundary-layer flow over local three-dimensional surface irregularities. *Trudy TsAGI* no. 2079, pp. 3–19. [In Russian.]

Makhankov, V. V. 1991 On discontinuous solutions in three-dimensional hypersonic interactive boundary layers. *Izv. Akad. Nauk SSSR, Mekh. Zhidk. Gaza* **2**, 19–26. [In Russian.]

Maskell, E. C. 1955 Flow separation in three dimensions. R. A. E. Rep. Aero. no. 2565.

Neiland, V. Ya. 1981 Asymptotic theory of separation and interaction between boundary layer and supersonic gas flow. *Usp. Mech.* **4**(2), 3–62. [In Russian.]

Neish, A. E. & Smith, F. T. 1992 On turbulent separation in the flow past a bluff body. *J. Fluid Mech.* **241**, 444–463.

Nickel, K. 1973 Prandtl's boundary-layer theory from the viewpoint of a mathematician. *A. Rev. Fluid Mech.* **5**, 405–428.

Nishioka, M. & Miyagi, T. 1978 Measurements of velocity distributions in the laminar wake of a flat plate. *J. Fluid Mech.* **84**, 705–715.

Peridier, V. J., Smith, F. T. & Walker, J. D. A. 1991*a* Vortex-induced boundary-layer separation. Part 1. The unsteady limit problem $Re \to \infty$. *J. Fluid Mech.* **232**, 99–131.

Peridier, V. J., Smith, F. T. & Walker, J. D. A. 1991*b* Part 2. Unsteady interacting boundary-layer theory. *J. Fluid Mech.* **232**, 133–165.

Prandtl, L. 1905 Über Flüssigkeitsbewegung bei sehr kleiner Reibung. In *Verh. d. III Int. Math.-Kongr., Heidelberg, Leipzig, Teubner*, pp. 484–491.

Raetz, G. S. 1957 A method of calculating three-dimensional laminar boundary layers of steady compressible flow. Northop Corp. Rep. no. NA1-58-73.

PHILOSOPHICAL TRANSACTIONS OF THE ROYAL SOCIETY A MATHEMATICAL, PHYSICAL & ENGINEERING SCIENCES

PHILOSOPHICAL TRANSACTIONS OF THE ROYAL SOCIETY A MATHEMATICAL, PHYSICAL & ENGINEERING SCIENCES

Downloaded from rsta.royalsocietypublishing.org

Ruban, A. I. 1981 Singular solution of the boundary layer equations which can be extended continuously through the point of zero surface friction, *Izv. Akad. Nauk SSSR, Mekh. Zhidk. Gaza* **6**, 42–52. [In Russian.]

Ruban, A. I. 1982*a* Asymptotic theory of short separation regions on the leading edge of a slender airfoil. *Izv. Akad. Nauk SSSR, Mekh. Zhidk. Gaza* **1**, 42–51. [In Russian.]

Ruban, A. I. 1982*b* On stability of preseparating boundary layer on the leading edge of a slender airfoil. *Izv. Akad. Nauk SSSR, Mekh. Zhidk. Gaza* **6**, 55–63. [In Russian.]

Ruban, A. I. 1990 Marginal separation theory. In *Separated flows and jets* (*Proc. IUTAM Symp.*), pp. 47–54. Springer-Verlag.

Smith, F. T. 1978 Three-dimensional viscous and inviscid separation of a vortex sheet from a smooth non-slender body. R. A. E. Tech. Rep. no. 78095.

Smith, F. T. 1982*a* On the high Reynolds number theory of laminar flows. *IMA J. appl. Math.* **28**(3), 207–281.

Smith, F. T. 1982*b* Concerning dynamic stall. *Aeronaut. Q.* **33**(4), 331–352.

Smith, F. T. 1984 Non-uniqueness in wakes and boundary layers. *Proc. R. Soc. Lond.* A **391**, 1–26.

Smith, F. T. 1986 Steady and unsteady boundary-layer separation. *A. Rev. Fluid Mech.* **18**, 197–220.

Smith, F. T. & Burggraf, O. R. 1985 On the development of large-sized short-scaled disturbances in boundary layers. *Proc. R. Soc. Lond.* A **399**, 25–55.

Smith, F. T. & Daniels, P. G. 1981 Removal of Goldstein's singularity at separation, in flow past obstacles in wall layers. *J. Fluid Mech.* **110**, 1–37.

Smith, F. T., Papageorgiou, D. & Elliott, J. W. 1984 An alternative approach to linear and nonlinear stability calculations at finite Reynolds numbers. *J. Fluid Mech.* **146**, 313–330.

Smith, F. T. & Walton, A. G. 1989 Nonlinear interaction of near-planar TS waves and longitudinal vortices in boundary-layer transition. *Mathematika* **36**, 262–289.

Stewartson, K. 1974 Multistructured boundary layers on flat plates and related bodies. *Adv. appl. Mech.* **14**, 145–239.

Stewartson, K. 1981 D'Alembert's paradox. *SIAM Rev.* **23**(3), 308–343.

Stewartson, K., Cebeci, T. & Chang, K. C. 1980 A boundary-layer collision in a curved duct. *Q. Jl Mech. appl. Math.* **33**, 59–75.

Stewartson, K. & Simpson, C. J. 1982 On a singularity initiating a boundary-layer collision. *Q. Jl Mech. appl. Math.* **35**, 1–16.

Stewartson, K., Smith, F. T. & Kaups, K. 1982 Marginal separation. *Stud. appl. Math.* **67**(1), 45–61.

Sychev, Vic. V. 1980 On some singular solutions of boundary layer equations on a moving surface. *Prikl. Math. Mekh.* **44**(5), 831–838. [In Russian.]

Sychev, V. V., Ruban, A. I., Sychev, Vic. V. & Korolev, G. L. 1987 *Asymptotic theory of separated flows*. Moscow: Nauka. [In Russian.]

Telionis, D. P. 1981 *Unsteady viscous flows*. Springer-Verlag.

Telionis, D. P. & Werle, M. J. 1973 Boundary-layer separation from downstream moving boundaries. *Trans. Am. Soc. Mech. Engrs J. appl. Mech.* **40**(2), 369–374.

Timoshin, S. N. 1991 Singularity in solution of three-dimensional boundary-layer equations due to wall jets collision. *Izv. Akad. Nauk SSSR, Mekh. Zhidk. Gaza* **4**, 75–81. [In Russian.]

Van Dommelen, L. L. & Cowley, S. J. 1990 On the Lagrangian description of unsteady boundary-layer separation. Part 1. General theory. *J. Fluid Mech.* **210**, 593–626.

Van Dommelen, L. L. & Shen, S. F. 1982 The genesis of separation. In *Numerical and physical aspects of aerodynamic flows* (ed. T. Cebeci), pp. 293–311. Springer-Verlag.

Vickers, I. P. 1992 Nonlinear effects in two-dimensional separating-flow transition. Ph.D. thesis, University of London.

Walton, A. G. & Smith, F. T. 1992 Properties of strongly nonlinear vortex/Tollmien–Schlichting-wave interactions. *J. Fluid Mech.* **224**, 649–676.

Wang, K. C. 1970 Three-dimensional boundary layer near the plane of symmetry of a spheroid at incidence. *J. Fluid Mech.* **43**, 187–209.

PHILOSOPHICAL TRANSACTIONS OF THE ROYAL SOCIETY A MATHEMATICAL, PHYSICAL & ENGINEERING SCIENCES

PHILOSOPHICAL TRANSACTIONS OF THE ROYAL SOCIETY A MATHEMATICAL, PHYSICAL & ENGINEERING SCIENCES

Downloaded from rsta.royalsocietypublishing.org

Wang, K. C. 1971 On the determination of the zones of influence and dependence for three-dimensional boundary-layer equations. *J. Fluid Mech.* **48**, 397–404.

Werle, M. J. & Davis, R. T. 1972 Incompressible laminar boundary layers on a parabola at angle of attack: a study of separation point. *Trans. Am. Soc. mech. Engrs J. appl. Mech.* **39**(1), 7–12.

Williams, J. C. & Johnson, W. D. 1974 Note on unsteady boundary-layer separation. *AIAA Jl* **12**(10), 1427–1429.

Zametaev, V. B. 1986 Existence and nonuniqueness of local separation zones in viscous jets. *Izv. Akad. Nauk SSSR, Mekh. Zhidk. Gaza* **1**, 38–45. [In Russian.]

Zametaev, V. B. 1987*a* Singular solution of the boundary-layer equations on a slender cone. *Izv. Akad. Nauk SSSR, Mekh. Zhidk. Gaza* **2**, 65–72. [In Russian.]

Zametaev, V. B. 1987*b* Local separation on a slender cone preceding vortex sheet development. *Izv. Akad. Nauk SSSR, Mekh. Zhidk. Gaza* **6**, 21–28. [In Russian.]

Zametaev, V. B. 1989 Formation of singularities in a three-dimensional boundary layer. *Izv. Akad. Nauk SSSR, Mekh. Zhidk. Gaza* **2**, 58–64. [In Russian.]

Zubarev, V. M. 1983 Boundary layer on a moving surface of a cylinder. *Izv. Akad. Nauk SSSR, Mekh. Zhidk. Gaza* **6**, 38–42. [In Russian.]

Received 8 March 1993; accepted 9 June 1993

PHILOSOPHICAL TRANSACTIONS OF THE ROYAL SOCIETY A MATHEMATICAL, PHYSICAL & ENGINEERING SCIENCES

PHILOSOPHICAL TRANSACTIONS OF THE ROYAL SOCIETY A MATHEMATICAL, PHYSICAL & ENGINEERING SCIENCES